CONTROLS OF BASEMENT FABRIC ON RIFT COUPLING AND DEVELOPMENT OF NORMAL FAULT GEOMETRIES: INSIGHTS FROM THE RUKWA – NORTH MALAWI RIFT

Erin Heilman[1]

Folarin Kolawole[2]

Estella A. Atekwana[3]*

Micah Mayle[1]

Mohamed G. Abdelsalam[1]

[1]*Boone Pickens School of Geology*
Oklahoma State University
Stillwater, Oklahoma, USA

[2]*ConocoPhillips School of Geology & Geophysics*
University of Oklahoma
Norman, Oklahoma, USA

[3]*Department of Geological Sciences*
College of Earth, Ocean, and Environment
University of Delaware
Newark, Delaware, USA

**Corresponding author email: atekwana@udel.edu*

August 2018

Highlights

- To the SW, newfound strike-slip fault links the Rukwa and North Malawi Rift (RNMRS)
- To the NE, RNMRS border faults, intervening faults and volcanic centers are colinear
- RNMRS border faults and transfer structures align with pre-existing basement fabrics
- Basement fabrics guide the development of normal fault geometries and rift bifurcation
- Basement fabrics facilitate the coupling of the RMRS border faults and transfer structures

ABSTRACT

The Rukwa Rift and North Malawi Rift Segments (RNMRS) both define a major rift-oblique segment of the East African Rift System (EARS), and although the two young rifts show colinear approaching geometries, they are often regarded as discrete rifts due to the presence of the intervening Mbozi Block uplift located in-between. This problem has been complicated by the dominance of the Rungwe volcanic features along the northeastern boundary of the Mbozi Block and lack of distinct normal faults along the southwestern boundary of the block. Here, we investigate the coupling of discrete rift segments during the onset of continental rifting, modulated by the control of pre-existing basement fabrics on the development of the border fault geometries and linkage across the intra-rift transfer zone. We utilized the Shuttle Radar Topography Mission Digital Elevation Models (SRTM-DEM) to investigate the morphological architecture of the rift domains; and aeromagnetic data and SRTM-DEM to assess the relationships between the rift structures and the pre-existing basement fabric (in plan-view). Our results show that the present-day morphology of the RNMRS is characterized by along-rift alternation of rift shoulder polarity, characteristic of coupled rift segments. Careful interpretation

of filtered aeromagnetic maps along the northeastern and southwestern boundaries of the RNMRS reveal striking alignment of the rift-bounding faults with colinear NW-SE-trending pre-existing basement fabrics. We find that rift coupling along the northeastern boundary of the Mbozi Block transfer zone is accommodated by magmatism utilizing pre-existing fault systems, whereas, coupling along the southwestern boundary is accommodated by a new-found dextral strike-slip fault. Additionally, we show how the configuration of the pre-existing basement fabrics may influence the development of rectilinear or curvilinear normal fault geometries (plan-view) along the rifts, and the formation of basin-scale rift bifurcation around basement inter-rift transfer zones. In summary, we suggest that the structural continuation of the boundary faults along the RNMRS, and their alignment with colinear basement fabrics demonstrate the influence of structural inheritance on the coupling and amalgamation of approaching rift segments.

1. INTRODUCTION

Pre-existing basement fabrics are often major facilitators of continental rifting environments. Mechanically, they represent areas of structural weakness that can become reactivated and allow rifts to propagate preferentially along them (e.g., Daly et al., 1989). Several studies have documented the relationships between rift faults and the pre-existing basement fabrics (e.g., Wheeler and Karson, 1989; Kinabo et al., 2007, 2008; Taylor et al., 2011; Phillips et al., 2016; Kolawole et al., 2018; Siuda et al., 2018). Further, recent studies have assessed the 3-dimensional relationship between pre-existing basement thrusts and intra-rift normal faults, revealing the control of the pre-existing basement structures on the nucleation and strain distribution along the normal faults (e.g., Collanega et al., 2018). In the Cenozoic East African Rift System (EARS), which is divided into an Eastern, a Western and a Southwestern Branch (Fig. 1A), several zones of well-developed basement fabric influence rifting. One of the best recently-documented examples highlighting the influence of the Precambrian basement shear zones on rifting in eastern Africa is the role of the Mwembeshi Shear Zone on the development of the Luangwa Rift (Fig. 1A; Sarafian et al., 2018). It was demonstrated that the Mwembeshi Shear Zone acted as lithospheric conduit for fluids to migrate up the lithosphere, thus facilitating the weakening and subsequent initiation of the Luangwa rift in the Permo-Triassic.

However, the relationship between rift segments along the western branch of the EARS and the Precambrian shear zones is rather complex and warrants detailed and careful examination. For example, the Precambrian NW-trending Aswa shear zone resulted in the termination (rather than facilitation) of the northeastward propagation of the Albertine-Rhino graben which represents the northern-most segment of the Western Branch (Katumwehe et al., 2015) (Fig. 1A). On a basin scale, previous studies have also shown that pre-existing basement

shear zones can influence the localization of fault development (e.g., Phillips et al., 2016; Kolawole et al., 2018), and in fact control fault segmentation and across-basin strain transfer at later stages of rift development (e.g., Muirhead and Kattenhorn, 2018).

The border faults along large continental rift systems, e.g., the EARS, are typically ~100 km long (e.g., Foster et al., 1997; Lao-Davila et al., 2015), and the development of such large normal faults with complex segment linkage styles are yet to be fully understood (e.g., Fossen and Rotevatn, 2016; Gawthorpe et al., 2003; Rotevatn et al., 2018). However, since the interactions between the large normal faults within juvenile extensional tectonic settings lead to the systematic coupling of rift segments across transfer zones (e.g., Corti, 2012), border fault segmentation, geometries and continuity between rift segments can provide insight into the larger process of coupling between the segments of a rift system.

In this study, we focus on the Rukwa-North Malawi segment of the EARS, which is a major rift-oblique segment of the rift system and serves as the central segment of the system. For simplicity, we here-in refer to the Rukwa - Northern Malawi Rift segment of the East African Rift as the "RNMRS". This segment is composed of the Rukwa Rift basin, the North Malawi Rift basin and the Mbozi Block which represents the accommodation zone between the two rifts (Fig. 1B). We address the longstanding question of the role of long-lived pre-existing basement structures in the development of the trends and geometries of rift-bounding faults, leading to subsequent coupling of individual rift segments during the onset of continental rifting. We demonstrate that there is continuous structural connectivity along the boundaries of the RNMRS, modulated by reactivation of the Precambrian metamorphic fabrics, and show that the characteristic plan-view geometries of the rift-bounding faults are modulated by the configuration of the basement fabric.

2. GEOLOGIC SETTING

2.1. The Precambrian Domains

The Rukwa-North Malawi Rift Segment is located within the NW-trending Paleoproterozoic Ubendian orogenic belt which is sandwiched between the Archean Tanzanian craton in the northeast and the Bangweulu cratonic block to the southwest (Figs. 2A-B; Fritz et al., 2013). The Ubendian Belt is composed of different Precambrian terranes bounded by steep shear zones (Delvaux et al., 2012). These terranes contain granulite-facies metamorphic rocks (2100-2025 Ma), amphibolite-facies metamorphic rocks and granitoids (1960-1800 Ma) that have undergone dextral strike-slip shearing and granitic plutons (1090-1120 Ma), (Fritz et al., 2013). The Paleoproterozoic Usagaran orogenic belt that extends NE-SW perpendicular to the Ubendian orogenic belt in southern Tanzania, is composed of eclogites (~2000 Ma), volcano-sedimentary cover with some low-grade metamorphism (~1920 Ma), and granitoids and granitoid gneisses (1900-1730 Ma) (Fritz et al., 2013). The Usagaran and Ubendian orogenic belts resulted from collision with the Tanzania craton, where the Usagaran orogenic belt was thrust onto the craton and the Ubendian orogenic belt was accreted along the craton's margin because of strike-slip motion (Daly, 1988; Lenoir et al., 1994). The Ubendian Belt was reactivated several times, first at ~1860 Ma as a shear zone, then again at ~800 Ma and was subsequently reactivated about every 200 Ma (Lenoir et al., 1994). Mapped shear zones along the Ubendian Belt include the ~600 km long and ~30 km-wide Mughese Shear Zone, the Mtose Shear Zone, and the Chisi Shear Zone (Fig. 2; Daly, 1988; Schenk et al., 2006; Delvaux et al., 2012). Recent studies have highlighted the role of the Mughese Shear Zone in fault development and the distribution of seismicity in Northern Malawi Rift Basin (Dawson et al. 2017; Kolawole et al., 2018).

188 *2.2. The Rukwa Rift, Northern Malawi Rift, and the Mbozi Block accommodation zone (RNMRS)*

189 The RNMRS evolved during the Permo-Triassic episode of rifting that affected southern and
190 eastern Africa, also known as Karoo rifting (Chorowicz, 2005). Outcrops of Karoo sediments
191 have been mapped along the southern end of the Rukwa Rift (Figure 2) and the northern section
192 of the North Malawi Rift Basin (Kilembe and Rosendahl, 1992). These sediments lie
193 unconformably over the Precambrian basement and consist mainly of sandstone, shale, and coal
194 and thicken towards the border faults providing evidence for reactivation of synthetic faulting in
195 the Permo-Triassic (Morley, 1992; Delvaux et al., 1992).

196 Cenozoic rifting began in the Upper Miocene, characterized by normal faulting and basin
197 subsidence with the diagenesis of Red Sandstones and Lake Bed Sediments (Delvaux and
198 Hanon, 1991). Additional subsidence occurred after the deposition of these packages, and in
199 different directions, evidenced by the drag orientations of sediment packages on the faults
200 (Kilembe and Rosendahl, 1992). The Cenozoic rifting featured the reactivation of older faults as
201 seen in seismic profiles of the Rukwa Rift in which the faults are mostly contiguous from Karoo
202 sediments to Red Sandstones to Lake Beds (Kervyn et al., 2006). The present-day tectonic
203 activity in the RNMRS consists of limited volcanic eruptions, minor seismicity in the Mbozi
204 Block region, and continued sedimentation in the Rukwa and North Malawi basins (Delvaux and
205 Hanon, 1991).

206 The present-day architecture of the RNMRS consists of the Rukwa Rift to the northwest
207 of the segment, with the Lupa Fault (generally considered the border fault) bounding it to the
208 northeast and the Ufipa Fault to the SW (Fig. 1B). Towards the southeastern end of the Rukwa
209 Rift. It bifurcates around the Mbozi Block forming the Songwe Trough (ST) to the northeast and
210 the Musangano Trough (MT) to the southwest. The Mbozi Block transitions into the North

Malawi Rift (also known as the North Basin) which represents the southeastern end of the RNMRS and it consists of a half-graben, bounded to the northeast by the Livingstone Fault (Fig. 1B). The Mbozi Block is referred to as an accommodation zone because it is thought to accommodate and transfer relative strain between the Rukwa and North Malawi Rift Basins (Delvaux and Hanon, 1993)

The Mbozi is a mass of Precambrian basement that is composed of Meta-basites and intermediate granulites and quartzites of the Mbozi Terrane (Daly, 1988) and is bounded to the southwestern by the Mughese Shear Zone (Fig. 2B), and overlain on the northeast by the volcanic deposits of the Rungwe Volcanic Province (RVP). The RVP is a ~1500 km^2 area of volcanic rocks and structures that evolved ca. 9 Ma (e.g., Fontijn et al., 2012), and a strong tectonic control on the localization of volcanic centers have been inferred (e.g., Fontijn et al., 2010, 2012). To the northeast of the RVP, a poorly defined NE-trending rift basin occurs, known as the "Usangu Basin", where Permo-Triassic to Recent sedimentary rocks overlie the Precambrian basement (Mbede, 2002).

The crustal thickness beneath the Rukwa Rift is ~37.5 km (Kim et al., 2009), but varies between ~33 km and ~39 km along the rift shoulder (Ufipa Plateau) (Hodgson et al., 2017), and increases slightly to 41.1–42.1 km in the northwestern-most part of the rift where the rifting is minimal. These suggest that overall, the crustal thinning beneath the rift has been minimal but may be slightly more beneath the Songwe Trough (Njinju et al., 2018). Camelbeeck and Iranga (1996) estimated ~42 km crustal thickness beneath the Songwe Trough. Whereas, an average crustal thickness of 39 km has been estimated for the Rungwe Volcanic Province, ~37-39 km for the North Malawi Rift, and 38-42 km for the Proterozoic terrains surrounding the North Malawi Rift (Borrego et al., 2016; Njinju et al., 2018).

2.3. Kinematics of the RNMRS

The mode of opening of the Rukwa Rift – Northern Malawi Rift segment is controversial. Overall, two models have been proposed. One of the models advocates for orthogonal rifting due to the dominance of NW-trending pre-existing basement fabric in the region, which resulted in the rotation of the E-W directed regional extension into NE-SW, thus producing NW-striking normal faults (e.g., Delvaux et al., 1992; Morley, 2010; Delvaux et al., 2012). The other model argues for oblique extension primarily due to the obliqueness of the rift segment to the E-W directed extension, thus resulting in the development of NW-trending dextral strike-slip faults (e.g., Chorowicz, 1989; Daly et al., 1989; Wheeler and Karson, 1994; Kervyn et al., 2006; Mortimer et al., 2007). Both models are based on observations from only the Rukwa Rift and North Malawi Rifts, and did not consider the kinematics of brittle structures along the Mbozi Block accommodation zone.

3.0 MATERIAL AND METHODS

In this study, we carried out detailed mapping of exposed and buried fault segments within the RNMRS. We utilized Shuttle Radar Topography Mission (SRTM) Digital Elevation Model (DEM) to locate surface expressions of faults; and filtered aeromagnetic data to map the plan-view trace of basement faults and metamorphic fabrics.

3.1. SRTM DEM Data

We extracted topographical profiles along the length of the rift from the SRTM DEM data to investigate surface morphology of the rift segments which could provide insight into the evolving nature of the rift architecture along the RNMRS.

3.2. Aeromagnetic Data

We combined three separate aeromagnetic surveys consisting of data acquired over northeastern Zambia, southern Tanzania and Northern Malawi. The Tanzania survey was collected between 1977-1980 with flight height of 200 m and a flight line spacing of 1 km. The Zambia survey was collected between 1973-1976 with a flight height of 150 m and a flight line spacing of 800-1000 m. The Malawi survey was carried out in 2013 with a flight height of 80 m, a flight line spacing of 250 m. Before merging the three surveys, we first corrected for the skewness of the data by reducing each of them to the magnetic pole (RTP). The RTP correction normalizes the magnetic field to the magnetic field at the pole so the anomalies retain their correct strike and shape, allowing the magnetic data to be interpreted as geologic structures (Baranov, 1957; Silva, 1986). Afterwards, we applied upward-continuation (Henderson and Zeitz, 1949) of 120 m to the RTP-corrected Malawi data, 50 m to the Zambia data in order to mathematically normalize the three datasets to a 200 m observational height. We then merged the three surveys into a single aeromagnetic grid file. Further, we applied the vertical derivative (VDR) filter to the merged data in order to enhance magnetic gradients associated with possible basement faults and basement metamorphic fabrics (Salem et al., 2008).

The vertical derivative edge filter has been very effective in the mapping of plan-view trace of buried active faults from aeromagnetic data in different parts of the EARS (Kinabo et al., 2007, 2008; Kolawole et al., 2017, 2018). Excluding the Rungwe Volcanic Province (RVP; Figure 3) where volcanic materials overlie the crystalline basement, there is no information on the presence of basaltic rocks along the fault segments interpreted in this study. Therefore, we assume induced magnetization as the primary source of magnetization, except in the Rungwe Volcanic Province (RVP) where volcanic deposits are present. However, we do not have

information on remanent magnetization in the RVP at this time. Due to the higher spatial resolution of the Malawi aeromagnetic data (62 m grid cell size) compared to those covering Zambia (225 m grid cell size) and Tanzania (250 m grid cell size), the magnetic anomalies are most significantly better resolved in the Malawi part of the filtered aeromagnetic maps.

4.0 RESULTS

4.1. Variation in rift morphology from topographic profiles

We examined fifteen rift-orthogonal topographic profiles (spaced at 40 km) along the RNMRS (Fig. 1B) to understand the overall along-strike variation in rift morphology. The investigation of rift dynamics by careful analyses of the topographic structures has provided important information on the subsurface architecture of rift systems (e.g., Pik et al., 2008; Wichura et al., 2011; Lao-Davila et al., 2015). Our morphological assessments focus on the variation in the scarp-heights (relief above the surface) of exposed normal faults along the RMNRS. This provides the minimum estimate of the relative vertical displacements of the faults at the point of assessment, hence the term 'exposed minimum vertical displacement' (EMVD) (Lao-Davila et al., 2015).

Profile 1 (Fig. 3), obtained at the northern tip of the Rukwa Rift shows no pronounced fault scarps, and the slight topographic high between Lake Tanganyika and Ufipa Fault represents the northernmost tip of the Ufipa Plateau. In Profile 2, the surface morphology of the rift shows sharp topographic gradients bounding the Rukwa Rift Valley. These topographic gradients correspond to the scarps of the Ufipa Fault (600 m) and the Lupa Fault (750 m). In this northern part of the Rukwa Rift, the Ufipa and Lupa Faults have comparable scarp heights, thus illustrating a typical graben structure. In Profile 3, the rift structure changes into a half-graben

surface morphology with the Ufipa Fault having a significantly higher escarpment than the Lupa Fault (~900 m difference). Profiles 4 to 7 show the same half-graben morphology for the Rukwa Rift as in Profile 3; however, we observe that the Ufipa Fault scarp is much higher than the topography of the Ufipa Plateau to its west along Profile 4.

Along Profiles 6 and 7, we observe that the Ufipa Fault scarp is lower than in the northern profiles (Profiles 1-5) and that the Lupa Fault scarp is also higher than in the northern profiles. In Profile 7, the Rukwa Rift splits into two basins separated by the Mbozi Block such that the west basin (Musangano Trough) is bound by the Ufipa Fault to the southwest, and the east basin (Songwe Trough) is bound by the Lupa Fault to the northeast. Profiles 7 to 9 shows a continuous southeastward decrease in the scarp heights of the Ufipa and Lupa Faults; and although the Ufipa Fault scarp is still visible south of the Mbozi Block along Profile 9, the Lupa Fault scarp is significantly diminished. Profile 9 shows a gentle topographic transition from the Musangano Trough to the Mbozi Block, but to the northeast of the Mbozi Block, the topography spikes abruptly, representing the northern limits of the Rungwe Volcanic Province (RVP). In Profile 10, the Ufipa Fault bounds what appears to be the southernmost extent of the Musangano Trough, while the uplifted Mbozi – RVP domain dominates the terrain and drops off into the Usangu Trough to the northeast. Profile 11 transects the northernmost tip of the North Malawi Rift, where the RVP (bounded to the northeast by the Livingstone Fault scarp) represents the most dominant structure in the terrain and the entire topography of the Mbozi Block and areas to its southwest are relatively lower.

Profiles 12 and 13 illustrate half-graben morphologies for the North Malawi Rift (North Basin) with the Livingstone Fault (northeast bounding fault) dominating the topography. Profile 14 transects the transfer zone between the North and Usisya Basins of the Malawi Rift showing

both the Livingstone border fault to the northeast and the Nyika Plateau to the southwest. Profile 15 which transects the Usisya Basin describes a half-graben surface morphology but in which the rift bounding fault is located on the southwest.

4.2. Aeromagnetic lineaments and basement fabric

The RTP merged (Fig. 4A) and edge-enhanced (Fig. 4B) aeromagnetic maps over the RNMRS provide a continuous plan-view image of the basement structures along the rift segment. Although the Malawi part of the merged data has the highest resolution, the moderate resolution of the Tanzania and Zambia parts of the data allows for considerable delineation of the trends of magnetic anomalies. Overall, the areas of basement exposures exhibit high amplitude, high frequency and short wavelength magnetic anomalies that delineate lineaments of interpretable trends (e.g., Kolawole et al., 2018). The high frequency lineaments can be easily observed on the rift shoulders of the Rukwa and North Malawi Rifts (Fig. 4B), and are commonly truncated at the rift margins by the rift-bounding faults (black arrows in Fig. 4B).

Within the rift valleys where sedimentary rocks overlie the deeply-buried basement rocks, the detailed magnetic fabric of the basement becomes suppressed such that gradients in the magnetic data could correspond to fault offset within the magnetic source (e.g., Grauch and Hudson, 2007, 2011; Kolawole et al., 2018) or remnants of the suppressed magnetic foliation of the source (Kolawole et al., 2018). In the study area, the magnetic anomalies within the rift basins are dominated by relatively lower amplitude, longer wavelength and lower frequency anomalies.

4.3. SRTM DEM Fault trends and Aeromagnetic lineaments

We compare the along-axis geometry of the rift-bounding faults (from SRTM DEM) with the metamorphic fabric (in plan view) of the host basement rocks along the rift shoulders (from filtered aeromagnetic data) (Figs. 5-11). Figures 5-9 focus on the southwestern boundary of the RNMRS, consisting of the Ufipa Fault of the Rukwa Rift, the southwestern boundary of the Mbozi Block and the southwestern boundary faults of the North Malawi Rift. Whereas, Figures 10 and 11 focus on the northeastern boundary of the RNMRS, consisting of the Lupa Fault of Rukwa Rift, the northeastern boundary of the Mbozi Block (i.e. the Rungwe Volcanic Province) and the Livingstone Fault of the North Malawi Rift. We constrain our identification of the Precambrian terranes and strike of their fabrics with previous field studies of the Precambrian basement along the RNMRS (e.g., Daly, 1988; Wheeler and Karson, 1989; Lenoir et al., 1994; Theunissen et al., 1996; Boven et al., 1999; Fernandez-Alonso et al., 2001; Ring et al., 2002; Schenk et al., 2006; Delvaux et al., 2012, Lawley et al., 2013; Kolawole et al., 2018). Overall, within the study area, we observe that the basement fabrics exhibit two styles, (1) discrete fabrics which include isolated magnetic lineaments of strong amplitude; and (2) distributed fabrics which encompass fabric sets of multiple medium-to-low amplitude magnetic lineaments as distributed fabrics.

4.3.1. Southwestern boundary of the RNMRS

In the northernmost part of SW Rukwa Rift (Chisi area) (Figs. 5A-C), we observe curvilinear fault geometries that follow Precambrian fabric (e.g., Ufipa, Chisi, Kalambo and Kanda Faults). In the Chisi area, the Rukwa Rift border fault consists of the Northern Ufipa Fault segment and the Chisi Fault segment. The tip of the Northern Ufipa Fault segment terminates against the

WNW-ESE Chisi Fault at a high angle (Fig. 5A). The Chisi Fault aligns with a strong WNW-ESE magnetic-high lineament (discrete fabric) (Fig. 5B-C) known as the Chisi Shear Zone, which extends eastward into the rift basin (Theunissen et al., 1996; Boven et al., 1999; Schenk et al., 2006; Fig. 2B). Also, the truncated Ufipa Fault segment aligns with the Ufipa Terrane basement fabrics (distributed fabrics). The North Ufipa Fault and Chisi Fault link at a very high angle to form a salient that point basinward (the Chisi Salient).

In the central part of the Ufipa Fault (Figs. 6A-C), the fault segments also exhibit curvilinear geometries and the hard linkage of major fault segments occur at high angles (e.g., Kwera relay ramp). The Kwera relay ramp is the largest relay zone along the Ufipa Fault. To the north of the Kwera relay ramp, the fault trends parallel to a magnetic lineament (discrete fabric) that is located to its east, whereas, to the west of this fault segment, the basement is characterized by two cross-cutting sets (NNW-SSE and NW-SE) of distributed fabrics. The NNW-SSE set represent the fabrics of the Ufipa Terrane, but the origin NW-SE is unknown at this time. The Ufipa Fault segments appear to follow the NNW-SSE basement fabrics but side-steps by means of short fault segments that align with the NW-SE fabric set. To the south of the relay ramp, the Ufipa Fault strikes parallel to the Mughese Shear Zone fabric which is colinear with the NNW-SSE set.

Towards the southern part of the Ufipa Fault, in Figures 7A-C, we observe that the Ufipa Fault segments exhibit rectilinear geometries such that it is difficult to delineate fault bends that could correspond to breached relay ramps. In addition, we observe a stronger alignment of the Ufipa Fault segments with the Mughese Shear Zone fabric within the area. To the east of the Ufipa Fault, a fault that strikes parallel to the Ufipa Fault separates the Musangano Trough from the Mbozi Block. The Mbozi basement is characterized by

metamorphic fabrics that strike WNW-ESE to NW-SE, oblique to the fault but in which subtle bends in the fault trend align with the basement fabric.

In the southern part of the Ufipa Fault (Figs. 8A-C), the fault is characterized by two segments. One of the segments represents a rectilinear southward continuation of the Ufipa Fault and is bounded to the east by a linear ridge that separates it from the Musangano Trough (see "Mughese Fault" segment at Tunduma in Figs. 8A-C). The other segment splays away from the former and delineates a curvilinear geometry that looks like those in the northern and central segments of the Ufipa Fault; this curvilinear segment bounds the southernmost part of the Musangano Trough (see "Ufipa Fault" in Figs. 8A-C). Around Kaseye town (see Fig. 8A), the basement is partially buried and more deeply buried around Chitipa to the south. The continuation of the Ufipa Fault is only evident in the aeromagnetic data as a strong magnetic-low lineament that is bounded by bands of magnetic-high lineaments (see magnetic fabrics around Kaseye town in Fig. 8B). Within the Kaseye area, the NW-striking Mughese Shear Zone fabrics are truncated by a discrete N-S trending magnetic-high lineament (see area within purple rectangle in Fig 8C). The magnetic-low lineament that projects as a southward continuation of the Ufipa Fault persists along the Mughese Shear Zone fabric into the Karonga area of the North Basin of Malawi Rift where the Mughese Shear Zone is abruptly truncated by the Karonga Fault (KF in Fig. 8C). The Mbozi Terrane fabric strike NW-SE, at low angles to the trend of the Mughese Shear Zone.

Detailed analyses of the onshore faults along the hinge zone of the Northern Malawi Rift (Karonga area) are well documented in Kolawole et al. (2018). Major onshore hinge zone faults include the Karonga Fault (KF), St. Mary Fault (SMF), Kaporo Fault (KPF), Lupaso Fault (LF), Katesula Fault (KTF) and the Mbiri Fault (Figs. 9A-C). Although the Karonga Fault cuts the

basement fabric, several basement-rooted buried fault segments along the rift margin align with the fabric of the Mughese Shear Zone (Kolawole et al., 2018). It is interesting to note that the Mbiri Fault, the longest fault (and potentially has the largest throw?) along the rift margin is sub-parallel to the strike of the continuation of the Ufipa Fault into the area ("Mughese Fault" in Fig. 9C). Although segments of the Mbiri Fault appear to align with the Mughese Shear Zone fabic, it is not clear if the fault reactivated the southwestern boundary of the shear zone or if the fault partially aligns with the fabric of the shear zone. However, we observe that for the most part, the side-steps along the Mbiri Fault align with the basement fabric.

4.3.2. Northeastern boundary of the RNMRS

In the northern part of the Lupa Fault, the fault trend defines long, rectilinear segments (Fig. 10A) and aligns with the Katuma Terrane, similar to those observed in the southern part of the Ufipa Fault where faults align with the trend of the Ufipa Terrane (Fig. 7). Although, the E-W trending fabric of the Usagaran Orogenic Belt dominates the aeromagnetic data along the northeastern Rukwa Rift shoulder (Fig. 10B), we also observe that closer to the Lupa Fault scarp, there are some lineaments that align with the fault. To the southwest of the Lupa Fault (within the rift valley), a strong magnetic-high lineament which correspond to the Chisi Shear Zone (see onshore continuation and outcrop of the shear zone in Fig. 5), strike sub-parallel to the trend of the Lupa Fault, but deviates more significantly southwards (Figs. 4B and 10).

The southern part of the Lupa Fault (between the Katuma Terrane and the Rungwe Volcanic Province) is characterized by curvilinear fault segments (Fig. 10 and 11). The Lupa Terrane fabrics are oriented WNW-ESE, oblique to the Lupa Fault trend (Figs. 11A-C). However, subtle steps along the curvilinear fault segments align with the Lupa Terrane fabrics.

In the Rungwe Volcanic Province (RVP), the magnetic lineaments strike NW-SE (Fig. 11B), similar to those of the Mbozi Terrane (8B and C), and are truncated to the west by a strong NNW-striking magnetic high lineament (white arrows in Fig. 11B). Furthermore, we observe that the volcanic centers align with NNW-striking magnetic gradient superimposed on the NW-striking fabrics (black arrows in Fig. 11B). South of the Rungwe Volcanic Province, segments of the Livingstone Fault system describe rectilinear geometries and align with strong magnetic-high lineaments (shear zone?) in the Upangwa Terrane.

5.0 DISCUSSION

5.1. Rift architecture

The present morphology of the RNMRS reflects the result of multiple episodes of rifting that have affected this part of eastern Africa i.e. a Permo-Triassic rifting episode (Karoo), a Cretaceous episode and the ongoing Cenozoic rifting episode (e.g., Castaing, 1991; Morley et al., 1992). The Rukwa Rift has been described as both a graben (e.g., Zhao et al., 1997) and half-graben (e.g., Kilembe and Rosendahl, 1992) bounded by the oppositely-dipping Ufipa and Lupa normal faults. The Lupa Fault is commonly regarded as the major border fault of the Rukwa Rift due to its larger throw of ~7 km (Peirce and Lipkov, 1988) relative to the Ufipa Fault (Fig. 12); however, it has also been shown that the Cretaceous and Cenozoic sediments in the rift thicken towards both faults (Fig. 12; Morley et al., 1992; Zhao et al., 1997). In this study, our topographical assessments (Fig. 3, profiles 1-7) show that the scarp height of the Ufipa Fault consistently exceeds that of the Lupa Fault through-out the rift segment, thus suggesting significant footwall uplift along the Ufipa Fault.

The significantly lower scarp-height of the Lupa Fault suggests either that it has not been very active in Cenozoic times or that it has been heavily eroded since the cessation of Mesozoic rifting. However, based on these observations, we interpret that in the earlier rifting episodes (especially in the Permo-Triassic Karoo episode), the Lupa Fault played the role of the major border fault such that the basin defines a typical half-graben geometry; but in the present Cenozoic phase of rifting, the Ufipa Fault appear to have been preferentially accommodating more strain. Therefore, we suggest that the Rukwa Rift is possibly transitioning into an asymmetric-graben geometry. An asymmetric-graben is a graben with EMVD greater on one border fault compared to the other one, such that the basin polarity has shifted to the fault with the greater 'exposed minimum vertical displacement' (EMVD) (Lao-Davila et al., 2015). The implications of the present Rukwa Rift morphology on the Lupa Fault may reflect temporal and spatial migration of strain accommodation from a previously dominant border fault into another one that has been previously less-dominant. This could possibly be explained by the Scholz and Contreras (1998) suggestion that when a rift-bounding fault attains some limiting offset, motion on the fault will cease, and strain will be transferred to a new fault.

5.2. The Southwestern Boundary of the RNMRS and relationships with Precambrian Basement Fabric

In the Chisi area, the Northern Ufipa Fault segment terminates against the Chisi Shear Zone along which the Chisi Fault segment developed. The termination of the Ufipa Fault at its intersection with this shear zone exemplifies one of the roles of pre-existing basement structures as temporal and/or spatial mechanical 'barriers' that arrest and delimit the continuous lateral propagation of a fault. Several studies on fracture propagation have demonstrated that fractures

are principally bifurcated, blunted, and/or arrested when they intersect discontinuities, stress barriers and/or rock layers of significantly-contrasting mechanical properties along their path of propagation (e.g., Helgeson and Aydin, 1991; Gudmundsson and Brenner, 2001; Zhang et al., 2007; Zhang and Jeffrey, 2008). Other examples of normal fault termination at long-lived basement shear zones include the case of the Albertine-Rhino Graben terminating at the Aswa Shear Zone (Katumwehe et al., 2015) and the Okavango Rift border faults against the Sekaka Shear Zone (Modisi et al., 2000). We suggest that both the reactivation of the Chisi Shear Zone into the Chisi Fault and termination of fault segments at the shear zone demonstrate the strong influence of the Chisi Shear Zone on the development of this part of the Rukwa Rift.

Although the northern segments of the Ufipa Fault align with the basement fabrics (Fig. 5B-C) and the southern segments show even stronger alignment with the NNW-SSE fabrics of the Ufipa Terrane and/or Mughese Shear Zone (Fig. 7), we find that the central segments of the fault show only partial alignment with this basement fabric (Fig. 6A-C). These observations imply that, although the Ufipa Fault is thought to have largely propagated along the Mughese Shear Zone (Fig. 2; Delvaux et al., 2012), there is stronger control of the Mughese Shear Zone and Ufipa Terrane fabrics on the fault development along its northern and southern segments than in the central part. We suggest that the partial control of these NNW-SSE fabrics on the central Ufipa Fault segments is due to the occurrence of a NW-SE basement fabric set on the Mughese Shear Zone and Ufipa Terrane fabric (Fig. 6). This may also explain the localization of the largest relay zone along the Ufipa Fault at its central segment.

The Tunduma-Kaseye area of Malawi, through the Misuku Mountains (Fig. 8A) constitute the southern boundary of the Mbozi Block. Although, the SRTM DEM shows that the sub-aerial expression of the Ufipa Fault dies out roughly mid-way between Tunduma and

Kaseye, the filtered aeromagnetic data reveals that in the subsurface, the fault continues across the Kaseye-Chitipa area as a distinct magnetic-low lineament that bounds the Mughese Shear Zone to the south and runs southeastwards into the Karonga area (Fig. 8B). Upon closer observation of the continuation of this strong magnetic-low lineament in the Kaseye-Chitipa area, we find that it cuts-across and offsets a N-S striking magnetic-high lineament which extends 80 km southwards into the Permo-Triassic Luangwa Rift in Zambia. We interpret this N-S lineament as a mafic dike that is possibly related to one of the earlier (Triassic or Cretaceous) episodes of rifting which are known to have been associated with extensive late-stage diking events in the Luangwa Rift (e.g., Van de Velde and De Waele, 1998) and Shire Graben in southern Malawi (Castaing, 1991). Sedimentary deposits in the Kaseye-Chitipa area resulted in the burial and lack of sub-aerial exposure of this structure, thus making this study the first revelation of its existence in Northwestern Malawi.

Our analyses of the geometry of the interpreted dike structure (Fig. 13A), here in referred to as the Chitipa Dike, shows a distinct difference in the geometry of the structure to the north where it is cut by the strong magnetic-low lineament (continuation of the Ufipa Fault) and to the south (farther away from the fault intersection). South of Chitipa (Fig. 13B), we observe that the north-trending dike describes a consistent left-stepping geometry which diminishes across the Chitipa town location and continues with a more rectilinear geometry northwards into the Mughese Shear Zone area. This side-stepping geometry is typical of vertical sheet intrusions and are related to either magma intrusion into pre-existing stepped joint systems (e.g., Baer, 1991) or near-surface stress rotations during magma intrusion (e.g., Fossen, 2010). In this study, the coincidence and strike of the dike-steps along the NW- to NNW- striking basement fabric may in

fact suggest the possible influence of pre-existing basement fabric on the stepping geometries of dike intrusions during their emplacement in host metamorphic rocks (Fig. 13B).

Further north, where the dike is cut by the continuation of the Ufipa Fault, the filtered aeromagnetic data shows the dike exhibiting consistent right-lateral offsets across NW-SE magnetic gradients (Fig. 13C). This clear distinction in the structural style of the dike south of Chitipa and in the north across the continuation of the Ufipa Fault, suggest that the contrasting structural styles are associated with different geological processes. In a summary, we interpret that along the southern boundary of the Mbozi Block, the continuation of the Ufipa Fault, which itself aligns with the Mughese Shear Zone fabric (Fig. 8B-C), is a right-lateral strike-slip fault that displaced a N-S trending Mesozoic (?) dike intrusion (Fig. 13C). We further interpret that this strike-slip fault reactivated the Precambrian Mughese Shear Zone at some time post-Cretaceous (i.e. related to the present Cenozoic rifting phase), and therefore refer to it as the "Mughese Fault". This interpretation is further supported by the change in the morphological expression of the Ufipa Fault from a typical single-scarp style into a narrow linear valley-ridge style in the Tunduma area in the SRTM DEM (see "linear ridge" in Fig. 8A). The observed linear valley-ridge geomorphology is typical of active strike-slip fault zones (e.g., McCalpin et al., 2009). In addition, previous field studies in the area (Delvaux et al., 2012) observed strike-slip displacement on rock outcrops at Tunduma and Mbozi Quarry ("Q" in Fig. 8A). Using the Chitipa Dike as a strain marker, we observe that the offsets increase northwards across multiple splays of the Mughese Fault and estimate that the displacement is maximum at the major Mughese Fault trace (northernmost extent of the strike-slip fault zone). Since mafic intrusions often produce magnetic anomalies larger than the actual size of the sources, it is practically impossible to estimate the true cumulative strike-slip displacement from the aeromagnetic data.

554 However, based on the lateral dike separation across the fault on our aeromagnetic data, we
555 estimate a minimum of 500 m strike-slip displacement along the Mughese Fault (Fig. 13C). In
556 Figure 14, we present a conceptual model that summarizes our interpretation of the Chitipa Dike
557 geometry and the interaction of the Mughese Fault with the dike.

558 In Tunduma area (Fig. 8A), the presence of discrete breaching of the linear ridge by
559 stream channels suggest that the strike-slip displacement along the Mughese Fault is most-likely
560 a short-lived event that occurred at some time in the past during the development of the RNMRS.
561 The curvilinear fault scarp adjacent to the Mughese Fault at Tunduma shows single-scarp
562 morphology (not linear-ridge morphology) typical of normal faults as seen on the other segments
563 of the Ufipa Fault. Therefore, we interpret this curvilinear fault scarp as a possible old segment
564 of the Ufipa Fault that was 'pirated' by the Mughese strike-slip fault; thus, suggesting a phase in
565 which the Ufipa Fault accommodated strike-slip displacement.

566 Along the southwest margin of the North Malawi Rift (Karonga area), the Mughese Fault
567 diffuses into a zone of wide-spread faulting where the southeast-ward bend of the Mughese
568 Shear Zone controls the development of the normal faults and recent seismicity along the basin
569 hinge margin (Fig. 9A-C) (Kolawole et al., 2018; Dawson et al., 2018). Further south of Karonga
570 town, the NNW-striking Mbiri Fault is the dominant fault structure in terms of its length (and
571 displacement?) along this part of the hinge zone of the North Malawi Rift. We do not observe
572 any direct spatial connectivity between the Mughese Fault and the Mbiri Fault. However, based
573 on the sub-parallel geometry of both faults and the structural dominance of the Mbiri Fault in the
574 area, we suggest that the Mbiri Fault could possibly represent a continuation of the Mughese
575 Fault into the hinge zone of the Malawi Rift North Basin. It is also important to note that the
576 Mbiri Fault is synthetic to the Livingstone border Fault. Following the observations and

interpretations above, we suggest that there exists a well-developed continuous connectivity of rift-related structures along the southwestern boundary of the RNMRS, facilitated by the extent of the Mughese Shear Zone and the Ufipa Terrane. Interestingly, the linking of the oppositely-dipping Ufipa and Mbiri Faults by the Mughese strike-slip fault describes a structure that, overall, is similar to that of the Morley et al. (1990) convergent-approaching normal fault system.

5.3. The Northeastern Boundary of the RNMRS and relationships with Precambrian Basement Fabric

The northern segment of the Lupa Fault exhibits clear alignment with the trend of the Katuma Terrane (Fig. 10) and with a few interpretable magnetic lineaments (likely due to low resolution of the aeromagnetic data). We also note that the Lupa Fault is sub-parallel to the Chisi Shear Zone in this area. Farther south of the Lupa Fault (Kapalala-Kanga area; Figs. 10 A-C), the fault segments occur at a high angle to the Usagaran Belt and Lupa Terrane fabrics, thus indicating an apparent lack of control of pre-existing basement fabric on the propagation of the southern Lupa Fault, except in the coincidence of the fault steps with the trend of the basement fabrics.

The southern segment of the Lupa Fault transitions into the Rungwe Volcanic Province (RVP) where surficial cover of volcanic deposits obscures the southward continuation of the Lupa Fault (Fig. 11A). In addition, the presence of mafic volcanic deposits in the RVP (e.g., Fontijn et al., 2012) makes it difficult to make a reliable interpretation of the magnetic fabric of the underlying Precambrian basement (Fig. 11B). However, we find that a distinct magnetic-high lineament aligns with the Mbaka Fault surface trace (white arrows in Figs. 11A and 11B). Also, the distribution of volcanic centers in the RVP show alignment with both the Mbaka Fault trace

and a subtle curvilinear gradient (black arrows in Fig. 11B). Further south, the curvilinear gradient connects with the Livingstone Fault, the northeastern border fault of the North Malawi Rift. This curvilinear gradient coincides with the location and extents of the so-called "Ngozi-Rungwe Line" of Fontijn et al. (2010), described as a buried fault system that served as a conduit for magmatic fluids to migrate to the surface volcanic vents. Therefore, although it is possible that the magnetic anomalies in this area are affected by remanent magnetization from the volcanic deposits, we interpret that this aeromagnetic gradient provides a possible subsurface evidence of the fault system (Ngozi-Rungwe Line) that connects the Lupa Fault and the Livingstone Fault across the RVP. The filtered aeromagnetic data and previous field studies (e.g., Wheeler and Karson, 1989) shows that the Livingstone Fault segments align with and reactivated the fabric of the Upangwa Terrane (Figs. 11B-C). The observations and interpretations above suggest that there exists a well-developed continuous connectivity of rift-related structures along the northeastern boundary of the RNMRS. However, the relationship between the basement fabric and the buried faults beneath the volcanic deposits remains unclear.

5.4. Implications for Rift Development

5.4.1. Rift Coupling

In the Rukwa Rift, the substantial dominance of the Ufipa Fault rift shoulder over that of the Lupa Fault may imply that the Ufipa Fault is the present-day active border fault of the Rukwa Rift. This proposition may be supported by the hypocentral location of the 1994 Mw5.9 Rukwa earthquake and its aftershoks with epicentral location in the northern part of the rift (Fig. 12; Zhao et al., 1997). The nodal planes of the earthquake focal mechanism solution are broadly consistent with the orientation of both the Lupa and Ufipa faults, and relative position of

aftershocks to the main shock is well determined (Fig. 12; Zhao et al., 1997). Considering the uncertainty range of the earthquakes, the spatial distribution of the aftershocks relative to the main shock delineates a sub-horizontal fault zone that most fits the subsurface projection of the Ufipa Fault (Fig. 12). In addition, field investigations of the Kwera relay ramp (see Fig. 6 for location) revealed features that indicate recent activity along the Ufipa Fault (Delvaux et al., 2012). Camelbeeck and Iranga (1996) observed several lower crustal seismicity in the Rukwa Rift with most of the events clustering beneath the Songwe Trough and the Rungwe Volcanic Province (southern parts of the rift; Fig. 1B). The locations of the clusters suggest activity along the southern Lupa Fault and Mbeya Range Fault. However, since the scarp height (and throw?) of the Ufipa Fault decreases southwards (Fig. 3), and the throw on the Lupa Fault increases southwards (and rapidly along the Songwe Trough) (Morley et al., 1992), we infer that the present border fault role of the Ufipa Fault excludes the southermost parts of the Rukwa Rift.

It has also been observed that the early stage of continental rifting is typically characterized by the development of along-axis alternating polarity of rift segments, rift border faults, uplifted rift flanks (e.g., Bosworth, 1985; Rosendahl, 1987; Hayward and Ebinger, 1996; Lao-Davila et al., 2015). The zones of polarity changes (transfer/accommodation zones) serve to transfer extensional strain between the rift segments and link the border faults which often have variable structural styles and geometries (e.g., Morley et al., 1990; Wilson, 1999). Within young continental rift settings, interactions between these large border faults lead to the systematic coupling of border faults and rift segments across the transfer zones, and subsequent growth of the rift system (e.g., Corti, 2012). Along the RNMRS, the alternating location of the of rift shoulder uplift (SW in Rukwa Rift and NE in North Malawi Rift), typical of coupled rift segments, suggest that the RNMRS can be considered a coupled rift segment. Further, our study

here shows that there is in fact, continuous structural continuation along the northeastern and southwestern margins of the RNMRS, typical of a coupled rift segment. Although, studies in the EARS and illustrations of its rift segments had always assumed this to be true, we hereby provide evidence supporting it, for the first time. In the West Antarctic rift system, the localization of recent volcanism along transverse structures within an accommodation zone (the Discovery accommodation zone) suggests active structural interactions between the flanking rift segments (Wilson, 1999). Therefore, we further suggest that the focusing of Neogene volcanism (e.g., Fontijn et al., 2010, 2012) along the northeastern boundary faults of the Mbozi accommodation zone (Fig. 15A) may be indicative of the ongoing coupling of the Rukwa and North Malawi Rift's northeastern border faults.

5.4.2. Rift Kinematics

Several studies have suggested that the development of the RNMRS has been dominated by dextral strike-slip kinematics (e.g., Chorowicz, 1989; Daly et al., 1989; Wheeler and Karson, 1994; Kervyn et al., 2006; Mortimer et al., 2007). However, analyses of fault architecture, fault-kinematics, paleostress and present-day earthquake focal mechanism solution in the Rukwa Rift show that the present-architecture of the rift largely developed within a pure extensional setting with extension direction orthogonal to the trend of the RNMRS (Morley, 2010; Delvaux et al., 2012). Furthermore, Delvaux et al. (2012) observed dextral strike-slip faulting along the fault systems bounding the Rukwa Rift, but concluded that the strike-slip event was transitory and was associated with an early Mesozoic transpressional event that resulted in the inversion of Karoo sediments. In this study, we observe the existence of a well-defined strike-slip fault bounding the SW margin of the Mbozi Block that reactivated the Precambrian Mughese Shear Zone. We also

observe lack of present-day activity along the strike-slip fault, and that this fault displaced a buried mafic dike with at least 500 m of dextral offset.

In the absence of chronological data on the mapped dike, we posit that the dike is most-likely associated with the widespread late-Karoo dike swarms observed in the Luangwa Rift and Shire Graben (southern Malawi) (Castaing, 1991; Van de Velde and De Waele, 1998). We refer to this strike-slip fault as the "Mughese Fault", and the buried dike as the "Chitipa Dike". The Chitipa Dike, presented for the first time in this work, may constitute the most excellent record of strike-slip kinematics along the RNMRS. Although, our results agree with Delvaux et al. (2012) in that the strike-slip faulting along the RNMRS was short-lived, we suggest that future geochronological analyses of this intrusion may provide the most-reliable constraint on the timing of strike-slip faulting event. It is also interesting to note that if the Mughese strike-slip fault is post-Karoo, its development represents a late reactivation of the Mughese Shear Zone in the evolution of the RNMRS. However, late reactivation of rift-oblique basement shear zones is not uncommon in rift basins (e.g., Muirhead and Kattenhorn, 2018).

Following the considerations above, we present cartoons of the RNMRS, illustrating the continuous structural connectivity along the northeast and southwest boundaries guided by the basement fabrics (Fig. 15B), and possible subsurface geometries and interactions of the domain-bounding structures (Fig. 15B-E). The inferred dominance of the Ufipa Fault in the northern and central parts of the Rukwa Rift (Fig. 12) suggest possible truncation of the Lupa Fault at depth, such that the load of the basin hanging wall block is being carried by the Ufipa Fault (Fig. 15B). However, seismic data is needed to confirm this interpretation. We illustrate a possible spatial relationship between the RVP magma pathways and the Mbozi Block bounding faults in Figure 15C. In Figure 15D-E, we show a generalized basin geometry and flip in border fault polarity

692 from the Malawi Rift North Basin to the Usisya Basin. Overall, we posit that, along the
693 northeastern boundary of the Mbozi Block transfer zone strain is accommodated by magmatism
694 utilizing pre-existing fault systems, whereas, along the southwestern boundary, strain is
695 accommodated by dextral strike-slip faulting.
696
697 *5.5. Control of basement fabrics on normal fault geometries*
698 Overall, along the border faults of the Rukwa Rift, we find that strongly-curvilinear normal fault
699 geometries (in plan-view) occur in three distinct settings. One, in areas where the basement
700 fabrics describe high curvatures (>15°) (e.g., in the Chisi area, northern segment of the Lupa
701 Fault; Fig. 5). Second, in areas of superposition of discordant sets of basement fabrics, in which
702 the overall fault strike is parallel to one of the sets and relay ramp breach-faults follow the other
703 fabric set that is oblique to the overall fault strike (e.g., central segment of Ufipa Fault; Fig. 6).
704 Third, in areas where the faults propagate at high-angle to the strike of the basement fabrics (e.g.,
705 in the Kapalala-Kanga area, southern segment of the Lupa Fault; Fig. 10). In general, along the
706 RNMRS, we find that in areas where the basement fabrics show low curvatures (<10°), the fault
707 segments tend to describe long, rectilinear geometries with narrow or almost unidentifiable
708 breached-relay zones (e.g., Southern Ufipa Fault, Fig. 7; Mughese Fault, Fig. 8; Livingstone
709 Fault, Fig. 11). We suggest that the control of rectilinear (<10° curvature) basement fabrics on
710 the propagation of normal faults may result in the development of rectilinear fault segments with
711 greater likelihood of occurrence of narrow relay ramps and tip-to-tip fault linkage.
712 Curvilinear normal faults have been observed at various scales and at different
713 extensional tectonic settings (Fossen and Rotevatn, 2016). However, the first order curvilinear
714 normal faults are typically characterized by segment boundaries with salients (cusps) that plunge

basin-ward e.g., Salt-lake salient and Transverse Mountain salients of the Wasatch Fault in Utah (Fig. 16A), and the Gullfaks salient in the North Sea (Fig. 16B) (Fossen and Rotevatn, 2016). Also, the reported curvilinear faults show characteristic basin-ward concave geometries. However, the South Oquirrh Mountains normal fault zone, although curvilinear (Wu and Bruhn, 1994), exhibits striking basin-ward convex geometry in which the cusps point into the footwall of the fault (Fig. 16A). Wu and Bruhn (1994) suggested that convex curvilinear geometry of the South Oquirrh Mountains normal fault zone developed by sequential propagation of the fault into its foot-wall, guided by linkage across smaller en-echelon faults created by the lateral shear components at the tips of the propagating fault. Here, in the Rukwa Rift, we observe both convex- and concave-curvilinear normal fault geometries along the Ufipa and Lupa Faults. The central Ufipa Fault (Fig. 6) and southern Lupa Fault (Kapalala-Mwambani area in Fig. 10A-C) exhibit convex-curvilinear normal fault geometries, whereas the northern Ufipa Fault and the Chisi Fault demonstrate concave-curvilinear fault geometries (linked at the Chisi salient) (Fig. 5). Also, we find striking similarities between the concave- and convex-curvilinear fault geometries of the Rukwa Rift (Fig. 16C) with those in the southern Malawi Rift (Fig, 16D), the Jurassic sedimentary sequence of the northern North Sea rift (Gullfaks area) (Fig. 16B), and the Provo-Salt Lake City area (Fig. 16A). As show in Figure 16D, the segments of the Bilila-Mtakataka Fault in southern Malawi Rift present excellent examples of convex-curvilinear normal fault geometries (Jackson and Blekinsop, 1997). Recent studies on the relationships between the basement fabrics and the Bilila-Mtakataka Fault segments (Johnson et al., 2018; Hodge et al., 2018) show that some of the segments appear to align with the distributed basement fabrics, while others cut across the basement fabrics.

737 Based on the observations above, we present conceptual models for the control of
738 various configurations of pre-existing basement fabrics on the development of curvilinear normal
739 fault plan-view geometries (Fig. 17). We show how discrete and distributed basement fabrics and
740 combinations of the two categories of fabrics can influence the plan-view geometry of normal
741 faults. However, there is need to better understand (1) the influence of the basement fabrics on
742 the geometries of curvilinear normal faults in 3-dimensions, (2) the influence of the extension
743 direction on the development of the observed curvilinear normal faults in areas where the
744 basement fabric present mechanical anisotropy.

745 Although, Fossen and Rotevatn (2016) provide evidence of subsidiary short-cut faulting
746 across a salient, suggesting an impending evolution of concave-curvilinear faults into rectilinear
747 faults, it is not yet clear if the model applies to convex-curvilinear normal faults since the two
748 styles of faults are geometrically different. However, the synthetic Bilila-Mtakataka and the
749 Chirobwe-Ncheu Faults (Fig. 16D) in southern Malawi Rift may provide some insight. Since the
750 Chirobwe-Ncheu Fault is older than the Bilila-Mtakataka Fault (Jackson and Blekinsop, 1997),
751 the rectilinear geometry of the Chirobwe-Ncheu Fault suggests that the apices of convex
752 curvilinear segments may likewise eventually get breached to form more-rectilinear fault
753 segments. Conversely, we observe the opposite of this model along the Lupa Fault, where the
754 more-rectilinear northern Lupa Fault has accommodated much less strain compared to its
755 curvilinear southern segment which has the most strain within the Rukwa Rift (Morley et al.,
756 1992). Therefore, we suggest that although the model of temporal progression from a curvilinear
757 to rectilinear fault geometry may apply to some large normal faults, it may not apply to others.
758
759

760 *5.6. Rift Bifurcation*

761 The basin scale splaying of the Rukwa Rift around the Mbozi Block into the Musangano
762 and Songwe Troughs (Fig. 1B) obviously represents a smaller-scale of rift bifurcation when
763 compared to the continental scale bifurcation of rift systems around microplates. Examples of
764 such continental-scale rift bifurcation include the branching of the East African Rift around the
765 Tanzania microplate into the western and eastern branches (Fig. 1A; e.g., Rosendahl, B.R., 1987;
766 Versfelt and Rosendahl, 1989), the Red Sea Rift around the Sinai microplate into the Gulf of
767 Suez Rift and Dead Sea Transform, and the South Atlantic Rift around the Sergipe microplate
768 into the Tucano-Recôncavo Rift and Sergipe-Alagoas Transform (e.g., Szatmari and Milani,
769 1999) (Figs. 18A-C). Based on scale distinction, we therefore refer to the continental rift-system
770 scale bifurcation as first (1^{st}) order rift bifurcation (Figs. 18A-C) and the rift-basin scale
771 bifurcation as second (2^{nd}) order rift bifurcation (Fig. 18D-F). Similar to the Rukwa Rift, 2^{nd}
772 order rift bifurcations are common along the East African Rift System. Examples include the
773 Southern Malawi Rift bifurcation around the Shire Horst, the Shire Graben bifurcation around
774 the Namalambo Horst, and the Albertine Graben bifurcation around the Rwenzori Block (Fig.
775 18B; e.g., Castaing, 1991; Koehn et al., 2008; Lao-Davila et al., 2015; Xue et al., 2017).

776 Regardless of scale, numerical models have showed that inherited structural
777 heterogeneity and lateral strength variations are key controls on rift bifurcation (e.g., Brune and
778 Autin, 2013; Brune et al., 2017). However, it appears that 1^{st} order bifurcations commonly occur
779 at the tip of pre-existing microcratonic blocks along the path of propagation of a continental rift
780 system (e.g., Fig. 18A). Also, 2^{nd} order bifurcations appear to occur at the transfer zones between
781 approaching rift segments, possibly due to a high tendency for the development of interfingering
782 fault blocks in the transfer zones between colinear approaching rift segments (Morley, 1995) and

783 lateral rotation of the trapped blocks in the transfer zones between overlapping approaching rift
784 segments (Koehn et al., 2008).

785 It is possible that the bifurcation of the Rukwa Rift around the Mbozi Block is related to
786 the location of the block within the transfer zone of the colinear approaching Rukwa and North
787 Malawi Rift segments. However, we suggest that the basement fabrics of the Ubendian Belt
788 around the Mbozi Block transfer zone could be playing a complementary role in facilitating and
789 guiding the intra-rift bifurcation of the Rukwa Rift around the block. Our filtered aeromagnetic
790 map (Fig. 4B) shows that the block is dominated by a WNW-ESE and N-S fabrics. According to
791 Daly (1988), the Meta-basites and intermediate granulites and quartzites of the Mbozi Block are
792 characterized by lineations that trend NE-SW. These observations, however, suggest that the
793 Mbozi Block fabrics strike at oblique to high-angles to the trend of the colinear fabrics of the
794 basement terranes bounding the Mbozi Block (Katuma-Upangwa Terranes to the northeast, and
795 those of the Ufipa Terrane to the southwest) and the main rift-bounding faults (the Lupa, Ufipa,
796 Livingstone and Mughese Faults) (Fig. 15A). Therefore, we suggest that the colinear fabrics of
797 the basement terranes surrounding the Mbozi Block which are already controlling the
798 propagation and linking of the rift-bounding faults may be playing a significant role in guiding
799 the bifurcation of the Rukwa Rift around the Mbozi Block (Figs. 4B, 7, 8 and 11).

800

801 **6.0 CONCLUSIONS**

802 Our topographic analyses of the morphology of the RNMRS and detailed study of the
803 relationships between the pre-existing basement fabric and rift-related faults provide, for the first
804 time, evidence supporting the coupling of the Rukwa and North Malawi Rift. Our topographic
805 analyses in the Rukwa Rift suggest that the Ufipa Fault is the present-day active border fault of

806 the rift. We find that the Ufipa fault is the dominant topographic feature in the northern part of
807 the RMNRS and diminishes as it encounters the Mbozi block where it becomes a strike slip fault
808 (Mughese Fault), at which point the border fault polarity flips and the Livingstone Fault is the
809 dominant fault in the southern part of the RNMRS.

810 Further, we demonstrate the continuity structures along the northeastern and
811 southwestern margins of the RNMRS. We show that this structural connectivity across the
812 Mbozi Block transfer zone between the rifts is guided by the pre-existing Precambrian terrane
813 fabrics and associated shear zones. We show that the coupling of the RNMRS along the
814 northeastern boundary of the Mbozi Block transfer zone is accommodated by magmatism along
815 the linking faults, whereas, coupling along the southwestern boundary is accommodated by
816 strike-slip faulting. Overall, we suggest that the continuation of the boundary faults along the
817 RNMRS, and their alignment with colinear Precambrian basement fabric and shear zones
818 indicate the influence of the pre-existing basement structures on the coupling and amalgamation
819 of approaching colinear rift segments. On the basin-scale bifurcation of the Rukwa Rift, we infer
820 that the discordance of the basement fabrics within the Mbozi Block transfer zone to those of the
821 basement terranes bounding it may have facilitated the development of intra-rift bifurcation of
822 the rift around the transfer zone.

823 Furthermore, we show the influence of pre-existing basement fabrics on the development
824 of the RNMRS as evidenced in the geometry, termination and kinematics of the rift-bounding
825 fault segments. Our observations suggest that curvilinear normal fault geometries developed in
826 areas where the basement fabrics are either curvilinear, composed of superposed sets of
827 differently-orientated fabrics, or not favorably oriented to the extensional stress field. Whereas,
828 long, rectilinear fault geometries with narrow or almost unidentifiable breached-relay zones

developed in areas where the pre-existing basement fabrics are roughly rectilinear, suggesting the greater likelihood of occurrence of tip-to-tip linkage of fault segments.

Finally, we present the existence of a buried Pre-Cenozoic strike-slip-faulted mafic dike, which we suggest is potentially the most excellent record of strike-slip kinematics along the RNMRS. We further suggest that future geochronological analyses of this intrusion may provide the most-reliable constraint on the timing of the controversial strike-slip faulting event along the RNMRS.

Acknowledgements

This work was partially supported by the National Science Foundation (NSF) grant EAR10-09988 (awarded to E.A. Atekwana). Also, we acknowledge the Oklahoma State University (OSU) for the Niblack Scholarship awarded to Erin Heilman. We thank the Geological Survey Department of Malawi for allowing us to purchase the 2013 aeromagnetic data used in this study. We also thank the Zambia Geological Survey for allowing us to purchase the aeromagnetic data used in this study. We thank South African Development Community (SADC) for providing the Tanzania aeromagnetic data used in this study. This is the Oklahoma State University Boone Pickens School of Geology contribution no. 2018-.

References

Baer, G., 1991. Mechanisms of dike propagation in layered rocks and in massive, porous sedimentary rocks. *Journal of Geophysical Research: Solid Earth*, *96*(B7), pp.11911-11929.

Baranov, V., 1957. A new method for interpretation of aeromagnetic maps: pseudo-gravimetric anomalies. *Geophysics*, *22*(2), pp.359-382.

Borrego, D.J., 2016. Crustal Structure of the Rungwe Volcanic Province and Region Surrounding the Northern Lake Malawi Rift Basin. MSc Thesis, Pennsylvania State University.

Bosworth, W., 1985. Geometry of propagating continental rifts. *Nature*, *316*(6029), p.625.

Boven, A., Theunissen, K., Sklyarov, E., Klerkx, J., Melnikov, A., Mruma, A. and Punzalan, L., 1999. Timing of exhumation of a high-pressure mafic granulite terrane of the Paleoproterozoic Ubende belt (West Tanzania). *Precambrian Research*, *93*(1), pp.119-137.

Brune, S. and Autin, J., 2013. The rift to break-up evolution of the Gulf of Aden: Insights from 3D numerical lithospheric-scale modelling. *Tectonophysics*, *607*, pp.65-79.

Brune, S., Corti, G. and Ranalli, G., 2017. Controls of inherited lithospheric heterogeneity on rift linkage: Numerical and analog models of interaction between the Kenyan and Ethiopian rifts across the Turkana depression. *Tectonics*, *36*(9), pp.1767-1786.

Camelbeeck, T. and Iranga, M.D., 1996. Deep crustal earthquakes and active faults along the Rukwa trough, eastern Africa. *Geophysical Journal International*, *124*(2), pp.612-630.

Castaing, C., 1991. Post-Pan-African tectonic evolution of South Malawi in relation to the Karroo and recent East African rift systems. *Tectonophysics*, *191*(1-2), pp.55-73.

870 Chorowicz, J., 1989. Transfer and transform fault zones in continental rifts: examples in the
871 Afro-Arabian rift system. Implications of crust breaking. *Journal of African Earth*
872 *Sciences (and the Middle East), 8(2-4)*, pp.203-214.
873 Chorowicz, J., 2005. The east African rift system. *Journal of African Earth Sciences*, *43*(1),
874 pp.379-410.
875 Collanega, L., Bell, R., Coleman, A.J., Lenhart, A. and Breda, A., 2018. How do intra-basement
876 fabrics influence normal fault growth? Insights from the Taranaki Basin, offshore New
877 Zealand. EarthArxiv, DOI: 10.31223/osf.io/8rn9u
878 Corti, G., 2012. Evolution and characteristics of continental rifting: Analog modeling-inspired
879 view and comparison with examples from the East African Rift System. *Tectonophysics*,
880 *522*, pp.1-33.
881 Daly, M.C., 1988. Crustal Shear Zones in Central Africa - A kinematic approach to Proterozoic
882 Tectonics. *Episodes*, *11*(1), pp.5-11.
883 Daly, M.C., Chorowicz, J. and Fairhead, J.D., 1989. Rift basin evolution in Africa: the influence
884 of reactivated steep basement shear zones. *Geological Society, London, Special*
885 *Publications*, *44*(1), pp.309-334.
886 Dawson, S.M., Laó-Dávila, D.A., Atekwana, E.A. and Abdelsalam, M.G., 2018. The influence
887 of the Precambrian Mughese Shear Zone structures on strain accommodation in the
888 northern Malawi Rift. *Tectonophysics*, *722*, pp.53-68.
889 Delvaux, D., and Hanon, M., 1991. Neotectonics of the Mbeya area, SW Tanzania. *Annual*
890 *report of the Royal Museum of Central Africa, Department of Geology and*
891 *Mineralogy*, *1992*, pp.87-97.

892 Delvaux, D., Kervyn, F., Macheyeki, A.S. and Temu, E.B., 2012. Geodynamic significance of
893 the TRM segment in the East African Rift (W-Tanzania): Active tectonics and paleostress
894 in the Ufipa plateau and Rukwa basin. *Journal of Structural Geology*, *37*, pp.161-180.
895 Delvaux, D., Levi, K., Kajara, R. and Sarota, J., 1992. Cenozoic paleostress and kinematic
896 evolution of the Rukwa–North Malawi rift valley (East African Rift System). *Bulletin des*
897 *Centres de Recherche Exploration-Production ElfAquitaine*, *16*, pp.383-406.
898 Fernandez-Alonso, M., Delvaux, D., Klerkx, J. and Theunissen, K., 2001. Structural link
899 between Tanganyika-and Rukwa-rift basins at Karema-Nkamba (Tanzania): basement
900 structural control and recent evolution. *Mus. Roy. Afr. Centr., Tervuren (Belgique), Dép.*
901 *Géol. Min., Rap. Ann*, pp.91-100.
902 Fontijn, K., Delvaux, D., Ernst, G.G., Kervyn, M., Mbede, E. and Jacobs, P., 2010. Tectonic
903 control over active volcanism at a range of scales: case of the Rungwe Volcanic
904 Province, SW Tanzania; and hazard implications. *Journal of African Earth Sciences*,
905 *58*(5), pp.764-777.
906 Fontijn, K., Williamson, D., Mbede, E. and Ernst, G.G., 2012. The Rungwe Volcanic Province,
907 Tanzania–A volcanological review. *Journal of African Earth Sciences*, *63*, pp.12-31.
908 Fossen, H., 2010. *Structural geology*. Cambridge University Press.
909 Fossen, H. and Rotevatn, A., 2016. Fault linkage and relay structures in extensional settings—A
910 review. *Earth-Science Reviews*, *154*, pp.14-28.
911 Foster, A., Ebinger, C., Mbede, E. and Rex, D., 1997. Tectonic development of the northern
912 Tanzanian sector of the East African Rift System. *Journal of the Geological*
913 *Society*, *154*(4), pp.689-700.

914 Fritz, H., Abdelsalam, M., Ali, K.A., Bingen, B., Collins, A.S., Fowler, A.R., Ghebreab, W.,
915 Hauzenberger, C.A., Johnson, P.R., Kusky, T.M. and Macey, P., 2013. Orogen styles in
916 the East African Orogen: a review of the Neoproterozoic to Cambrian tectonic
917 evolution. *Journal of African Earth Sciences*, *86*, pp.65-106.
918 Gawthorpe, R.L., Jackson, C.A.L., Young, M.J., Sharp, I.R., Moustafa, A.R. and Leppard, C.W.,
919 2003. Normal fault growth, displacement localisation and the evolution of normal fault
920 populations: the Hammam Faraun fault block, Suez rift, Egypt. *Journal of Structural*
921 *Geology*, *25*(6), 883-895.
922 Grauch, V.J.S. and Hudson, M.R., 2007. Guides to understanding the aeromagnetic expression of
923 faults in sedimentary basins: Lessons learned from the central Rio Grande rift, New
924 Mexico. *Geosphere*, *3*(6), pp.596-623.
925 Grauch, V.J.S. and Hudson, M.R., 2011. Aeromagnetic anomalies over faulted strata. *The*
926 *Leading Edge*, *30*(11), pp.1242-1252.
927 Gudmundsson, A. and Brenner, S.L., 2001. How hydrofractures become arrested. *Terra*
928 *Nova*, *13*(6), pp.456-462.
929 Hayward, N.J. and Ebinger, C.J., 1996. Variations in the along-axis segmentation of the Afar
930 Rift system. *Tectonics*, *15*(2), pp.244-257.
931 Helgeson, D.E. and Aydin, A., 1991. Characteristics of joint propagation across layer interfaces
932 in sedimentary rocks. *Journal of Structural Geology*, *13*(8), pp.897-911.
933 Henderson, R.G. and Zietz, I., 1949. The upward continuation of anomalies in total magnetic
934 intensity fields. *Geophysics*, *14*(4), pp. 517-534.

935 Hodge, M., Fagereng, Å., Biggs, J., and Mdala, H., 2018.. Controls on early-rift geometry: New
936 perspectives from the Bilila-Mtakataka fault, Malawi. *Geophysical Research Letters, 45*,
937 3896–3905.
938 Hodgson, I., Illsley-Kemp, F., Gallacher, R.J., Keir, D., Ebinger, C.J. and Mtelela, K., 2017.
939 Crustal structure at a young continental rift: A receiver function study from the
940 Tanganyika Rift. *Tectonics*, *36*(12), pp.2806-2822.
941 Jackson, J. and Blenkinsop, T., 1997. The Bilila-Mtakataka fault in Malaŵi: An active, 100-km
942 long, normal fault segment in thick seismogenic crust. *Tectonics*, *16*(1), pp.137-150.
943 Johnson, S., Mendez, K., Beresh, S.C.M., Mynatt, W.G., Elifritz, E.A., Laó-Dávila, D.A.,
944 Atekwana, E.A., Abdelsalam, M.G., Chindandali, P.R.N., Chisenga, C. and Gondwe, S.,
945 2017.. The Relationships of Subparallel Synthetic Faults and Pre-existing Structures in
946 the Central Malawi Rift. *AGU Fall Meeting poster number T22C-03*.
947 Katumwehe, A.B., Abdelsalam, M.G. and Atekwana, E.A., 2015. The role of pre-existing
948 Precambrian structures in rift evolution: The Albertine and Rhino grabens,
949 Uganda. *Tectonophysics*, *646*, pp.117-129.
950 Kervyn, F., Ayub, S., Kajara, R., Kanza, E. and Temu, B., 2006. Evidence of recent faulting in
951 the Rukwa rift (West Tanzania) based on radar interferometric DEMs. *Journal of African*
952 *Earth Sciences*, *44*(2), pp.151-168.
953 Kilembe, E.A. and Rosendahl, B.R., 1992. Structure and stratigraphy of the Rukwa
954 rift. *Tectonophysics*, *209*(1-4), pp.143-158.
955 Kim, S., Nyblade, A.A. and Baag, C.E., 2009. Crustal velocity structure of the Rukwa Rift in the
956 western branch of the East African Rift system. *South African Journal of Geology*, *112*(3-
957 4), pp.251-260.

Kinabo, B.D., Atekwana, E.A., Hogan, J.P., Modisi, M.P., Wheaton, D.D. and Kampunzu, A.B., 2007. Early structural development of the Okavango rift zone, NW Botswana. *Journal of African Earth Sciences*, *48*(2), pp.125-136.

Kinabo, B.D., Hogan, J.P., Atekwana, E.A., Abdelsalam, M.G. and Modisi, M.P., 2008. Fault growth and propagation during incipient continental rifting: Insights from a combined aeromagnetic and Shuttle Radar Topography Mission digital elevation model investigation of the Okavango Rift Zone, northwest Botswana. *Tectonics*, *27*(3).

Koehn, D., Aanyu, K., Haines, S. and Sachau, T., 2008. Rift nucleation, rift propagation and the creation of basement micro-plates within active rifts. *Tectonophysics*, *458*(1-4), pp.105-116.

Kolawole, F., Atekwana, E.A., Laó-Dávila, D.A., Abdelsalam, M.G., Chindandali, P.R., Salima, J. and Kalindekafe, L., 2018. Active deformation of Malawi Rift's North Basin hinge zone modulated by reactivation of pre-existing Precambrian shear zone fabric. *Tectonics*, *37*, pp.683–704.

Lao-Davila, D.A., Al-Salmi, H.S., Abdelsalam, M.G. and Atekwana, E.A., 2015. Hierarchical segmentation of the Malawi Rift: The influence of inherited lithospheric heterogeneity and kinematics in the evolution of continental rifts. *Tectonics*, *34*(12), pp.2399-2417.

Lawley, C.J., Selby, D., Condon, D.J., Horstwood, M., Millar, I., Crowley, Q. and Imber, J., 2013. Lithogeochemistry, geochronology and geodynamic setting of the Lupa Terrane, Tanzania: implications for the extent of the Archean Tanzanian Craton. *Precambrian Research*, *231*, pp.174-193.

979 Lenoir, J.L., Liégeois, J.P., Theunissen, K. and Klerkx, J., 1994. The Palaeoproterozoic
980 Ubendian shear belt in Tanzania: geochronology and structure. *Journal of African Earth*
981 *Sciences, 19*(3), pp.169-184.
982 Mbede, E.I., 2002. Interpretation of refelction seismic data from the Usangu Basin, East African
983 Rift System. *Tanzania Journal of Science, 28*(1), pp.83-97.
984 McCalpin, J.P., Rockwell, T.K. and Weldon II, R.J., 2009. Paleoseismology of Strike-Slip
985 Tectonic Environments. *International Geophysics, 95*, pp.421-496.
986 Modisi, M.P., Atekwana, E.A., Kampunzu, A.B. and Ngwisanyi, T.H., 2000. Rift kinematics
987 during the incipient stages of continental extension: Evidence from the nascent Okavango
988 rift basin, northwest Botswana. *Geology, 28*(10), pp.939-942.
989 Morley, C.K., 1995. Developments in the structural geology of rifts over the last decade and their
990 impact on hydrocarbon exploration. *Geological Society, London, Special*
991 *Publications*, *80*(1), pp.1-32.
992 Morley, C.K., 2010. Stress re-orientation along zones of weak fabrics in rifts: An explanation
993 for pure extension in 'oblique' rift segments?. *Earth and Planetary Science*
994 *Letters*, *297*(3), pp.667-673.
995 Morley, C.K., Cunningham, S.M., Harper, R.M. and Wescott, W.A., 1992. Geology and
996 geophysics of the Rukwa rift, East Africa. *Tectonics, 11*(1), pp.69-81.
997 Morley, C.K., Nelson, R.A., Patton, T.L. and Munn, S.G., 1990. Transfer zones in the East
998 African rift system and their relevance to hydrocarbon exploration in rifts (1). *AAPG*
999 *Bulletin, 74*(8), pp.1234-1253.

1000 Mortimer, E., Paton, D.A., Scholz, C.A., Strecker, M.R. and Blisniuk, P., 2007. Orthogonal to
1001 oblique rifting: effect of rift basin orientation in the evolution of the North basin, Malawi
1002 Rift, East Africa. *Basin Research*, *19*(3), pp.393-407.
1003 Muirhead, J.D. and Kattenhorn, S.A., 2018. Activation of preexisting transverse structures in an
1004 evolving magmatic rift in East Africa. *Journal of Structural Geology*, *106*, pp.1-18.
1005 Njinju, E.A., Atekwana, E.A., Stamps, D.S., Abdelsalam, M.G., Atekwana, E.A., Mickus, K.L.,
1006 Kolawole, F. and Nyalugwe, V., 2018. Lithospheric Structure of the Malawi Rift:
1007 Implications for Rifting Processes in Magma Poor Rift Systems. *EarthArXiv*, DOI:
1008 10.31223/osf.io/83qd9
1009 Peirce, J.W. and Lipkov, L., 1988. Structural interpretation of the Rukwa rift, Tanzania.
1010 *Geophysics*, *53*(6), pp.824-836.
1011 Phillips, T.B., Jackson, C.A., Bell, R.E., Duffy, O.B. and Fossen, H., 2016. Reactivation of
1012 intrabasement structures during rifting: A case study from offshore southern
1013 Norway. *Journal of Structural Geology*, *91*, pp.54-73.
1014 Pik, R., Marty, B., Carignan, J., Yirgu, G. and Ayalew, T., 2008. Timing of East African Rift
1015 development in southern Ethiopia: Implication for mantle plume activity and evolution of
1016 topography. *Geology*, *36*(2), pp.167-170.
1017 Ring, U., Kröner, A., Buchwaldt, R., Toulkeridis, T. and Layer, P.W., 2002. Shear-zone patterns
1018 and eclogite-facies metamorphism in the Mozambique belt of northern Malawi, east-
1019 central Africa: implications for the assembly of Gondwana. *Precambrian*
1020 *Research*, *116*(1), pp.19-56.
1021 Rosendahl, B.R., 1987. Architecture of continental rifts with special reference to East
1022 Africa. *Annual Review of Earth and Planetary Sciences*, *15*(1), pp.445-503.

1023 Rotevatn, A., Jackson, C.A.L., Tvedt, A.B.M., Bell, R. and Blækkan, I., 2018. How do normal
1024 faults grow?. EarthArXiv.
1025 Salem, A., Williams, S., Fairhead, J.D., Ravat, D. and Smith, R., 2007. Tilt-depth method: A
1026 simple depth estimation method using first-order magnetic derivatives. *The Leading*
1027 *Edge*, *26*(12), pp.1502-1505.
1028 Sarafian, E., Evans, R.L., Abdelsalam, M.G., Atekwana, E., Elsenbeck, J., Jones, A.G. and
1029 Chikambwe, E., 2018. Imaging Precambrian lithospheric structure in Zambia using
1030 electromagnetic methods. *Gondwana Research*, *54*, pp.38-49.
1031 Schenk, V., Boniface, N., Loose, D., Alkmim, F.F. and Noce, C.M., 2006. Paleoproterozoic
1032 subduction zones at the margins of the Tanzania and Congo Cratons: evidence from
1033 eclogites with MORB-type chemistry in the Usagaran–Ubendian Belts of Tanzania and
1034 the Nyong complex of Cameroon. *The Paleoproterozoic Record of the São Francisco*
1035 *Craton*, pp.102-103.
1036 Scholz, C.H. and Contreras, J.C., 1998. Mechanics of continental rift
1037 architecture. *Geology*, *26*(11), pp.967-970.
1038 Silva, J.B., 1986. Reduction to the pole as an inverse problem and its application to low-latitude
1039 anomalies. *Geophysics*, *51*(2), pp.369-382.
1040 Siuda, K., Magee, C., Bell, R., Jackson, C.A.L. and Collanega, L., 2018. Pre-existing basement
1041 thrusts influence rifting in the Taranaki Basin, New Zealand. EarthArXiv.
1042 Szatmari, P. and Milani, E.J., 1999. Microplate rotation in northeast Brazil during South Atlantic
1043 rifting: Analogies with the Sinai microplate. *Geology, 27*(12), pp.1115-1118.

1044 Taylor, B., Weiss, J.R., Goodliffe, A.M., Sachpazi, M., Laigle, M. and Hirn, A., 2011. The
1045 structures, stratigraphy and evolution of the Gulf of Corinth rift, Greece. *Geophysical*
1046 *Journal International, 185*(3), pp.1189-1219.
1047 Theunissen, K., Klerkx, J., Melnikov, A. and Mruma, A., 1996. Mechanisms of inheritance of
1048 rift faulting in the western branch of the East African Rift, Tanzania. *Tectonics*, *15*(4),
1049 pp.776-790.
1050 Van de Velde, P., and De Waele, B., 1998. Geology of the Mupamadzi River area. Explanation
1051 of degree sheet 1231, SW quarter, Report No. 105, *Geological Survey Department,*
1052 *Republic of Zambia.*
1053 Versfelt, J. and Rosendahl, B.R., 1989. Relationships between pre-rift structure and rift
1054 architecture in Lakes Tanganyika and Malawi, East Africa. *Nature*, *337*(6205), p.354.
1055 Wheeler, W.H. and Karson, J.A., 1989. Structure and kinematics of the Livingstone Mountains
1056 border fault zone, Nyasa (Malawi) Rift, southwestern Tanzania. *Journal of African Earth*
1057 *Sciences (and the Middle East)*, *8*(2-4), pp.393-413.
1058 Wheeler, W.H. and Karson, J.A., 1994. Extension and subsidence adjacent to a "weak"
1059 continental transform: An example from the Rukwa rift, East Africa. *Geology*, *22*(7),
1060 pp.625-628.
1061 Wichura, H., Bousquet, R., Oberhänsli, R., Strecker, M.R. and Trauth, M.H., 2011. The Mid-
1062 Miocene East African Plateau: a pre-rift topographic model inferred from the
1063 emplacement of the phonolitic Yatta lava flow, Kenya. *Geological Society, London,*
1064 *Special Publications, 357*(1), pp.285-300.
1065 Wilson, T.J., 1999. Cenozoic structural segmentation of the Transantarctic Mountains rift flank
1066 in southern Victoria Land. *Global and Planetary Change*, *23*(1-4), pp.105-127.

Wu, D. and Bruhn, R.L., 1994. Geometry and kinematics of active normal faults, South Oquirrh Mountains, Utah: implication for fault growth. *Journal of Structural Geology*, *16*(8), pp.1061-1075.

Xue, L., Gani, N.D. and Abdelsalam, M.G., 2017. Geomorphologic proxies for bedrock rivers: A case study from the Rwenzori Mountains, East African Rift system. *Geomorphology*, *285*, pp.374-398.

Zhang, X. and Jeffrey, R.G., 2008. Reinitiation or termination of fluid-driven fractures at frictional bedding interfaces. *Journal of Geophysical Research: Solid Earth*, *113*(B8).

Zhang, X., Jeffrey, R.G. and Thiercelin, M., 2007. Deflection and propagation of fluid-driven fractures at frictional bedding interfaces: a numerical investigation. *Journal of Structural Geology*, *29*(3), pp.396-410.

Zhao, M., Langston, C.A., Nyblade, A.A. and Owens, T.J., 1997. Lower-crustal rifting in the Rukwa graben, East Africa. *Geophysical Journal International*, *129*(2), pp.412-420.

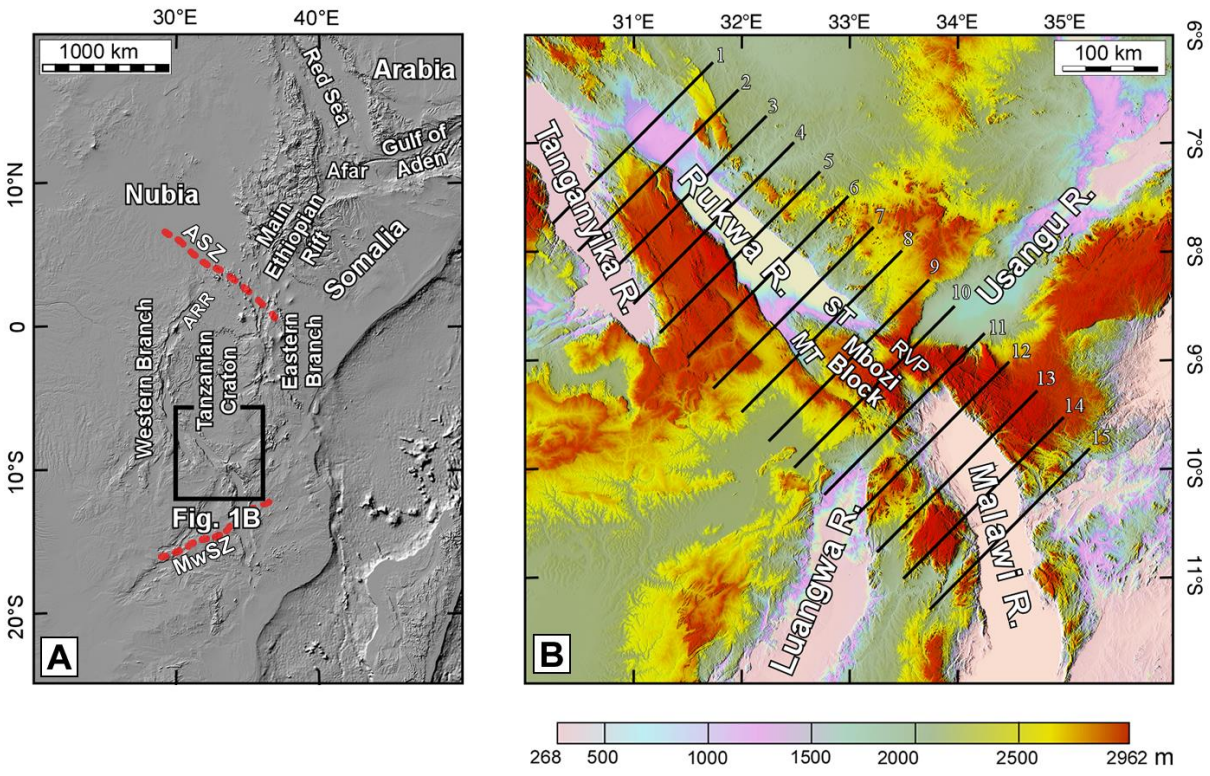

Fig.1. (A) Topographic map of the East African Rift System, showing the segments of the rift system and the location of the Rukwa-North Malawi Rift Segment (RNMRS) (black square). (B) Digital Elevation Model (DEM) of the RNMRS showing the different domains. Solid black lines represent topographic profile lines shown in Figure 3. ARR= Albertine-Rhino Rift, ASZ= Aswa Shear Zone, MT= Musangano Trough, MwSZ= Mwembeshi Shear Zone, RVP= Rungwe Volcanic Province, ST= Songwe Trough.

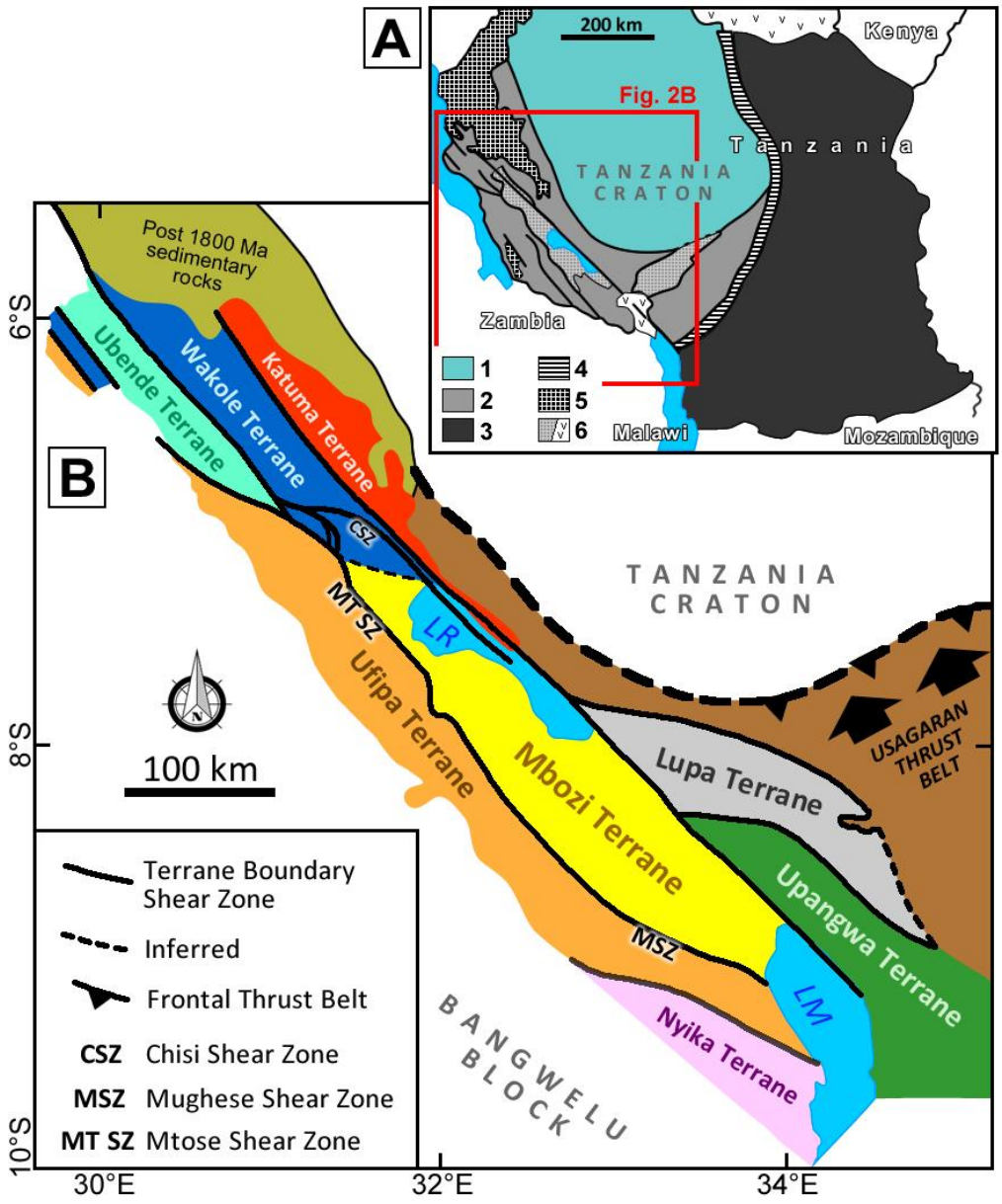

Fig. 2. (A) Precambrian domains around the Tanzanian Craton (modified after Theunissen et al., 1996; Boven et al., 1999; Fernandez-Alonso et al., 2001; Schenk et al., 2006). 1 = Archean craton; 2 = Paleoproterozoic Usagaran and Ubendian orogenic belts; 3 = Mozambique orogenic belt; 4 = western limit of Pan-African influence; 5 = Meso and/or Neoproterozoic sediments *(only for the Ubendian Belt region)*; 6 = Phanerozoic volcanics and sedimentary rocks. (B) Regional geological map of southwest Tanzania showing the terrane structure of the Ubendian orogenic belt within which the Rukwa-Malawi Rift Segment (RNMRS) developed.

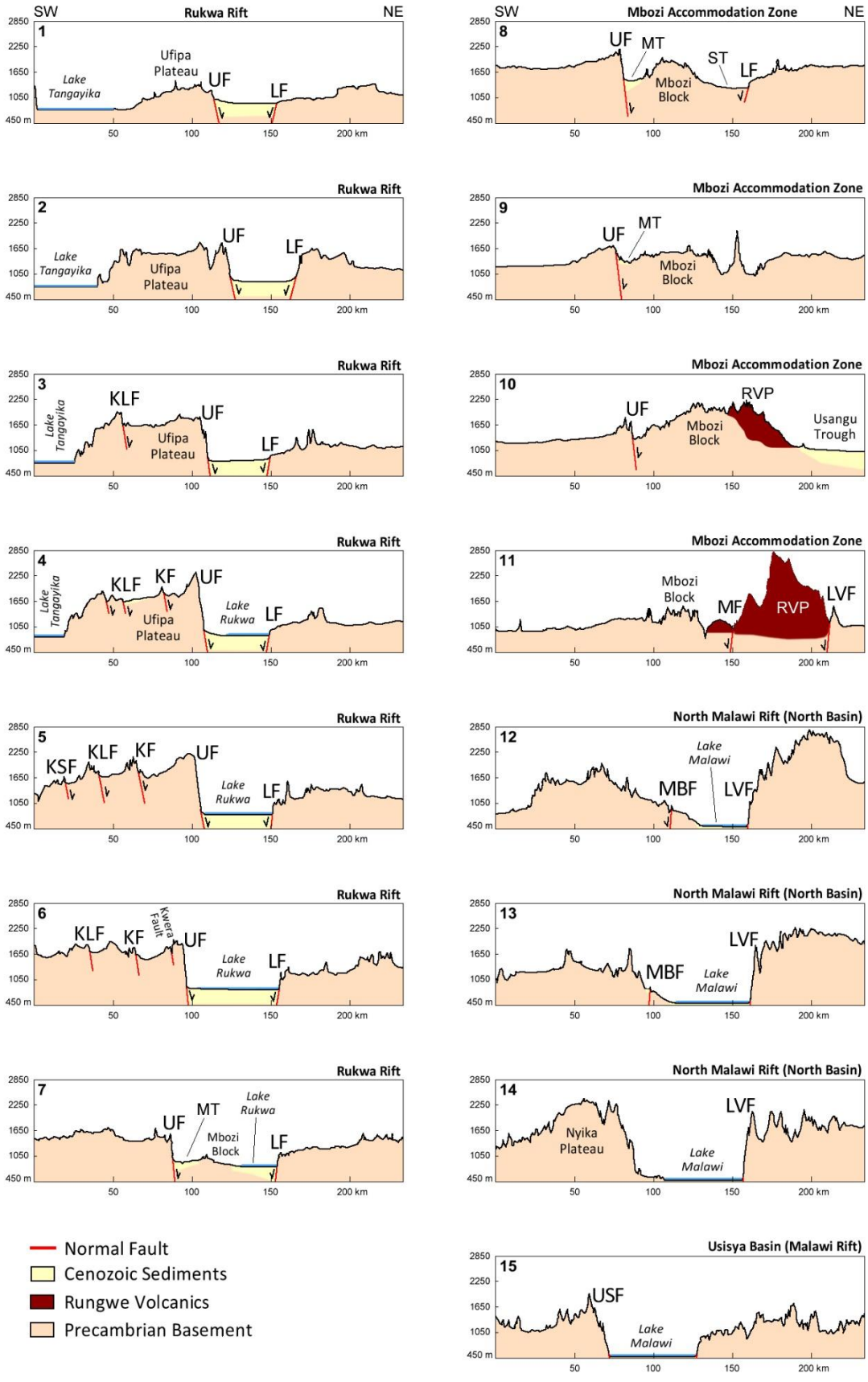
SW
Rukwa Rift
NE
1
Lake Tangayika
Ufipa Plateau
UF
LF
2
3
KLF
4
KF
Lake Rukwa
5
KSF
6
Kwera Fault
7
MT
Mbozi Block
SW
Mbozi Accommodation Zone
NE
8
ST
9
10
RVP
Usangu Trough
11
MF
LVF
North Malawi Rift (North Basin)
12
Lake Malawi
MBF
13
14
Nyika Plateau
Usisya Basin (Malawi Rift)
15
USF
2850
2250
1650
1050
450 m
50
100
150
200 km
Normal Fault
Cenozoic Sediments
Rungwe Volcanics
Precambrian Basement

Fig. 3. Topographic profiles across the Rukwa - North Malawi Rift segment. Profile numbers correspond to the profiles in Figure 1B. KLF = Kalambo Fault, KF = Kanda Fault, KSF = Kasanga Fault, LF = Lupa Fault, LVF = Livingstone Fault, MB = Mbozi Block, MBF = Mbiri Fault, MF = Mbaka Fault, MT = Musangano Trough, RVP = Rungwe Volcanic Province, ST = Songwe Trough, UF = Ufipa Fault, USF = Usisya Fault.

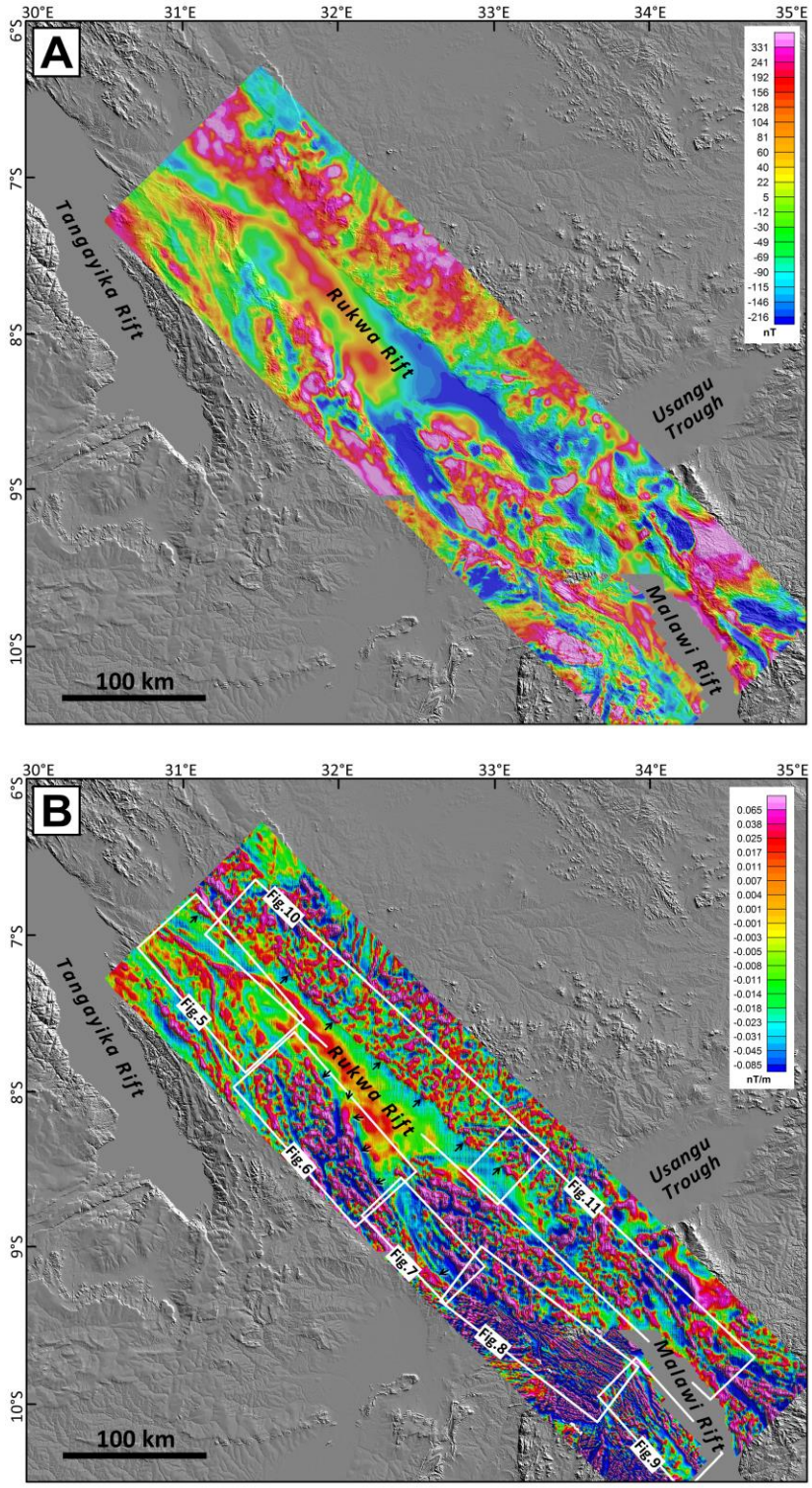

Fig. 4. (A) The reduced to pole Total Magnetic Intensity (RTP-TMI) map of the Rukwa-North Malawi Rift area, draped over the topographic digital elevation model of SW Tanzania. (B) The 1st vertical derivative map of the RTP-TMI map of the Rukwa-North Malawi Rift area draped over the topographic digital elevation model.

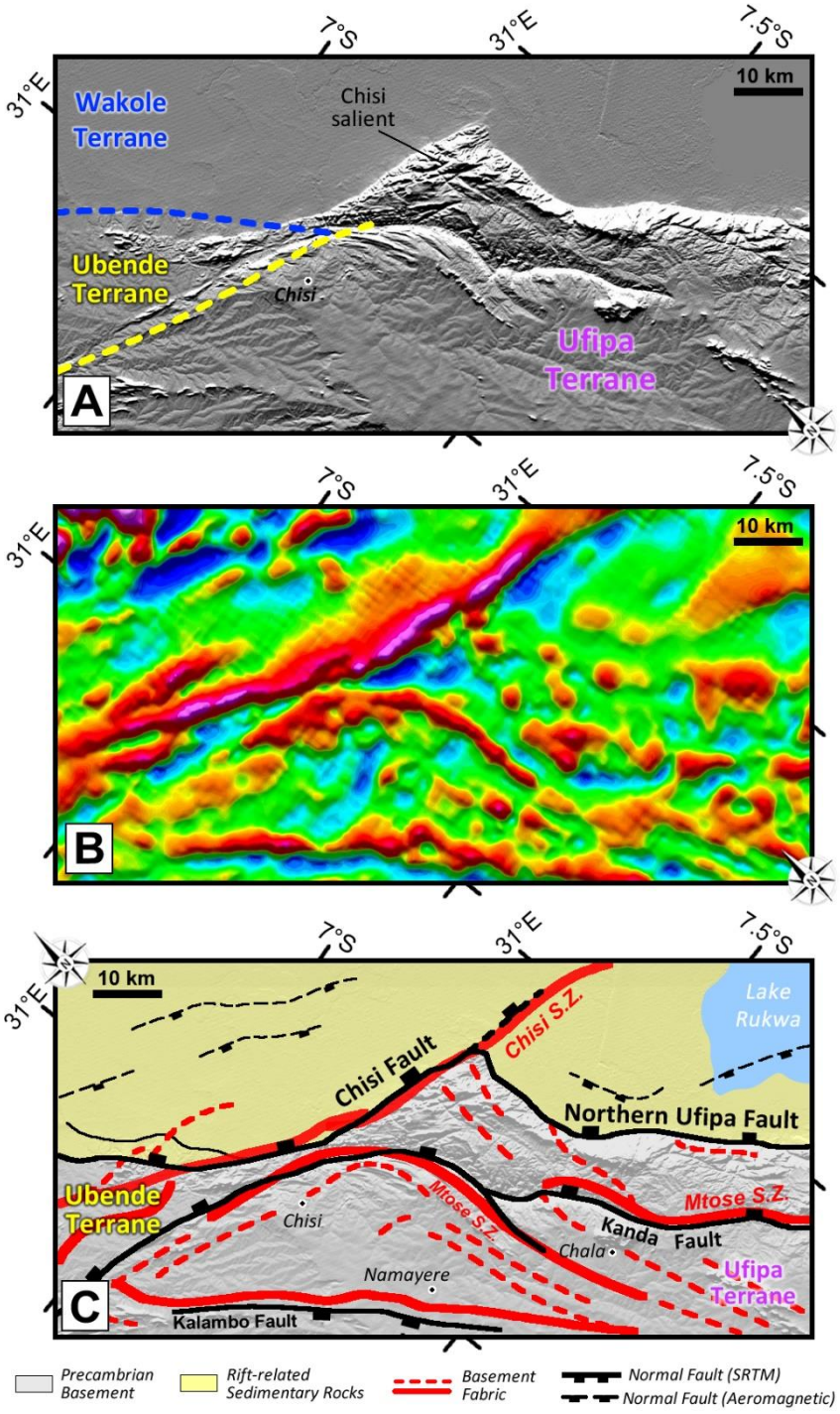

Fig. 5. Northernmost part of the Ufipa Fault, the SW boundary fault of the Rukwa Rift. Topographic digital elevation model in the top panel (A), the vertical derivative of the magnetic data in the middle panel (B), and a structural interpretation in the bottom panel (C).

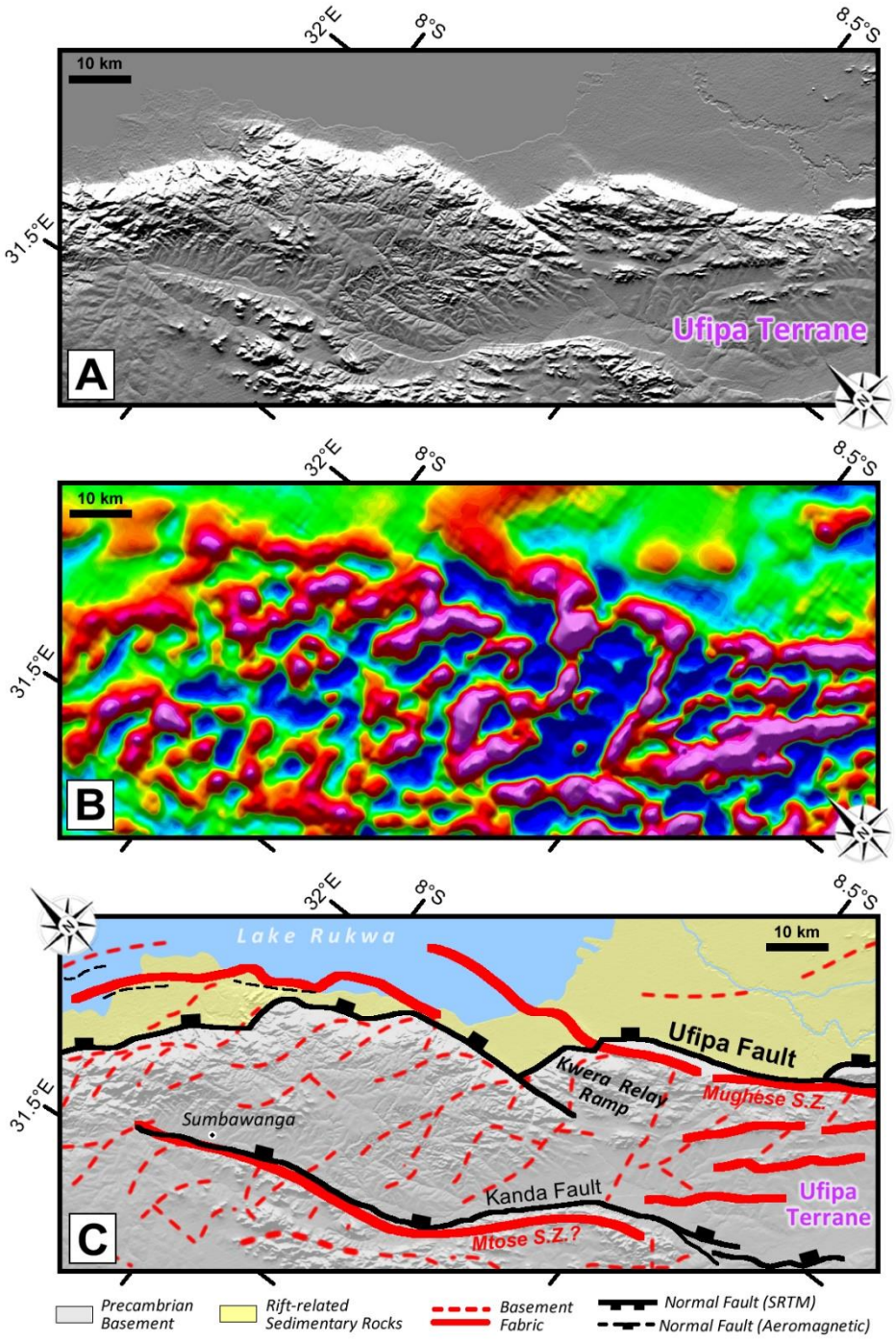

Fig. 6. Central segment of the Ufipa Fault, SW boundary of the Rukwa Rift. Topographic digital elevation model in the top panel (A), the vertical derivative of the magnetic data in the middle panel (B), and a structural interpretation in the bottom panel (C).

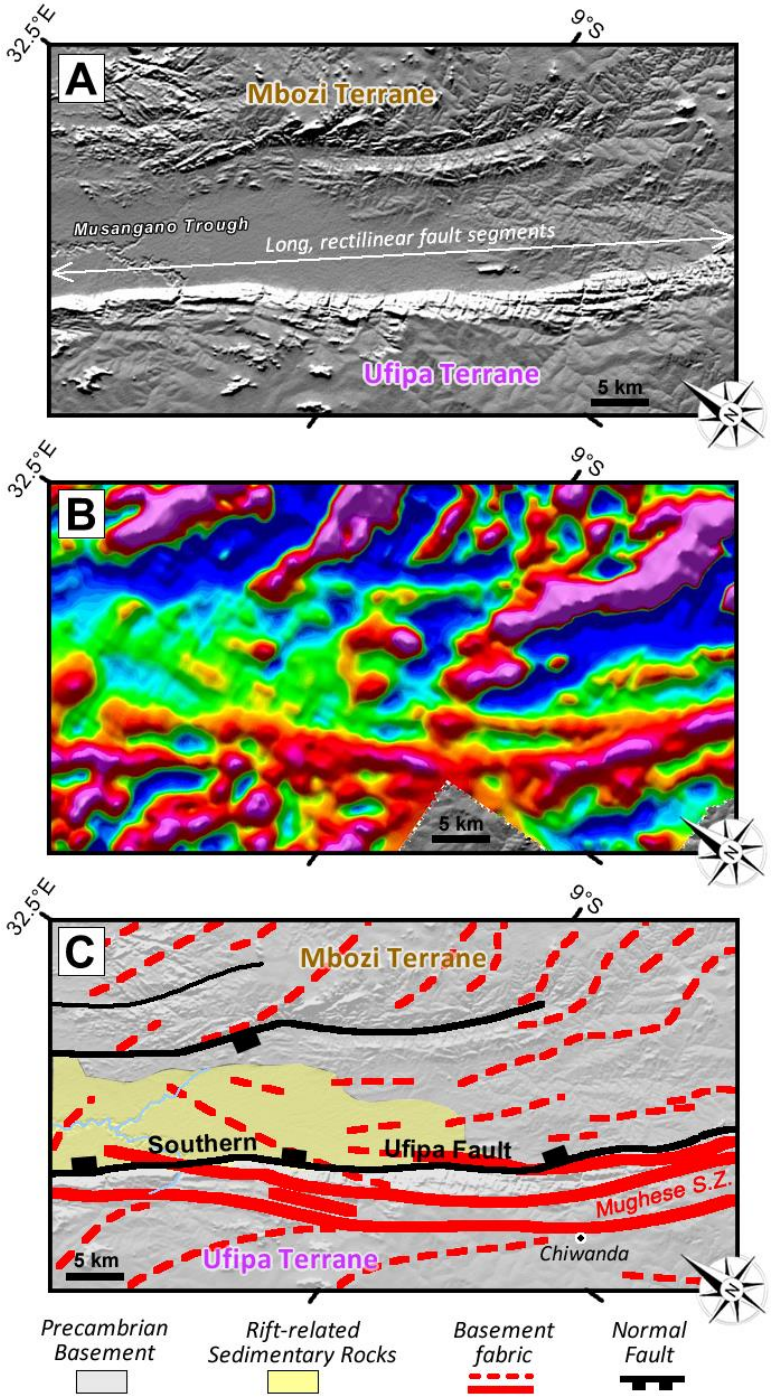

Fig. 7. The Musangano Trough part of the SW boundary of the Rukwa Rift. Topographic digital elevation model in the top panel (A), the vertical derivative of the magnetic data in the middle panel (B), and a structural interpretation in the bottom panel (C).

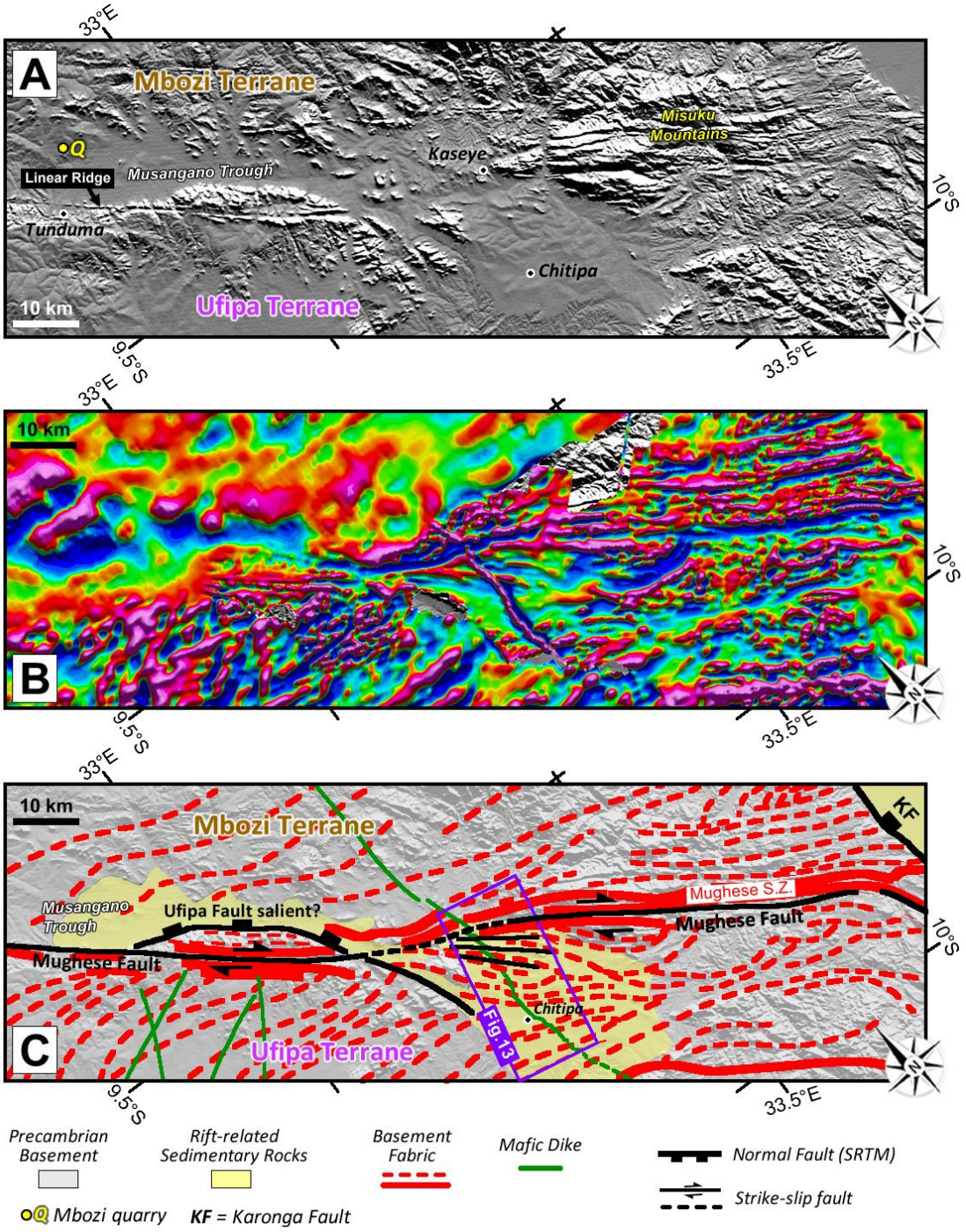

Fig. 8. The SW margin of the Mbozi Block. Topographic digital elevation model in the top panel (A), the vertical derivative of the magnetic data in the middle panel (B), and a structural interpretation in the bottom panel (C).

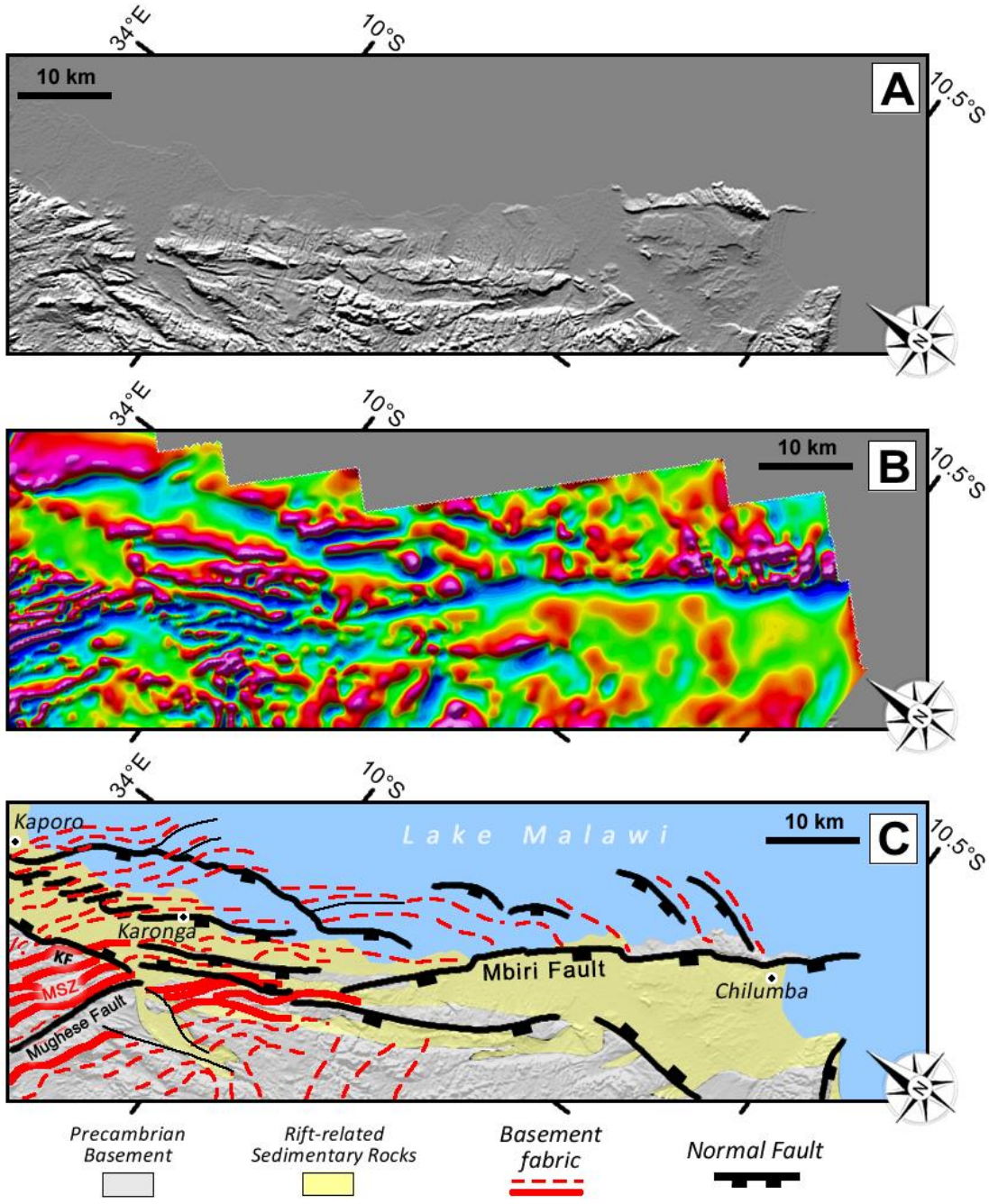

Fig. 9. The SW margin of the North Malawi Rift Basin (Karonga area). Topographic digital elevation model in the top panel (A), the vertical derivative of the magnetic data in the middle panel (B), and a structural interpretation in the bottom panel (C). MSZ = Mughese Shear Zone, KF = Karonga Fault. Fault and basement fabric interpretations from Kolawole et al. (2018).

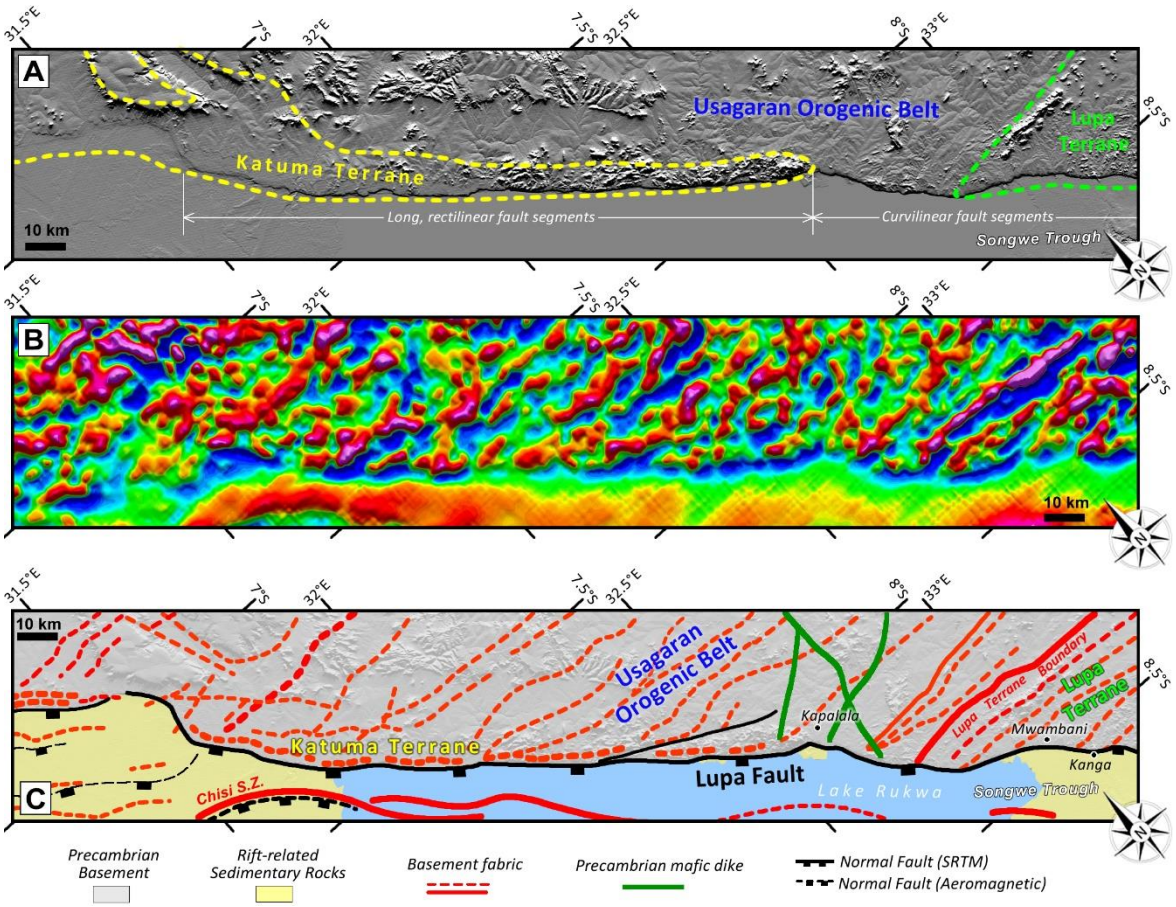

Fig. 10. The northern section of the Lupa Fault, the NE boundary fault of the Rukwa Rift. Topographic digital elevation model in the top panel (A), the vertical derivative of the magnetic data in the middle panel (B), and a structural interpretation in the bottom panel (C).

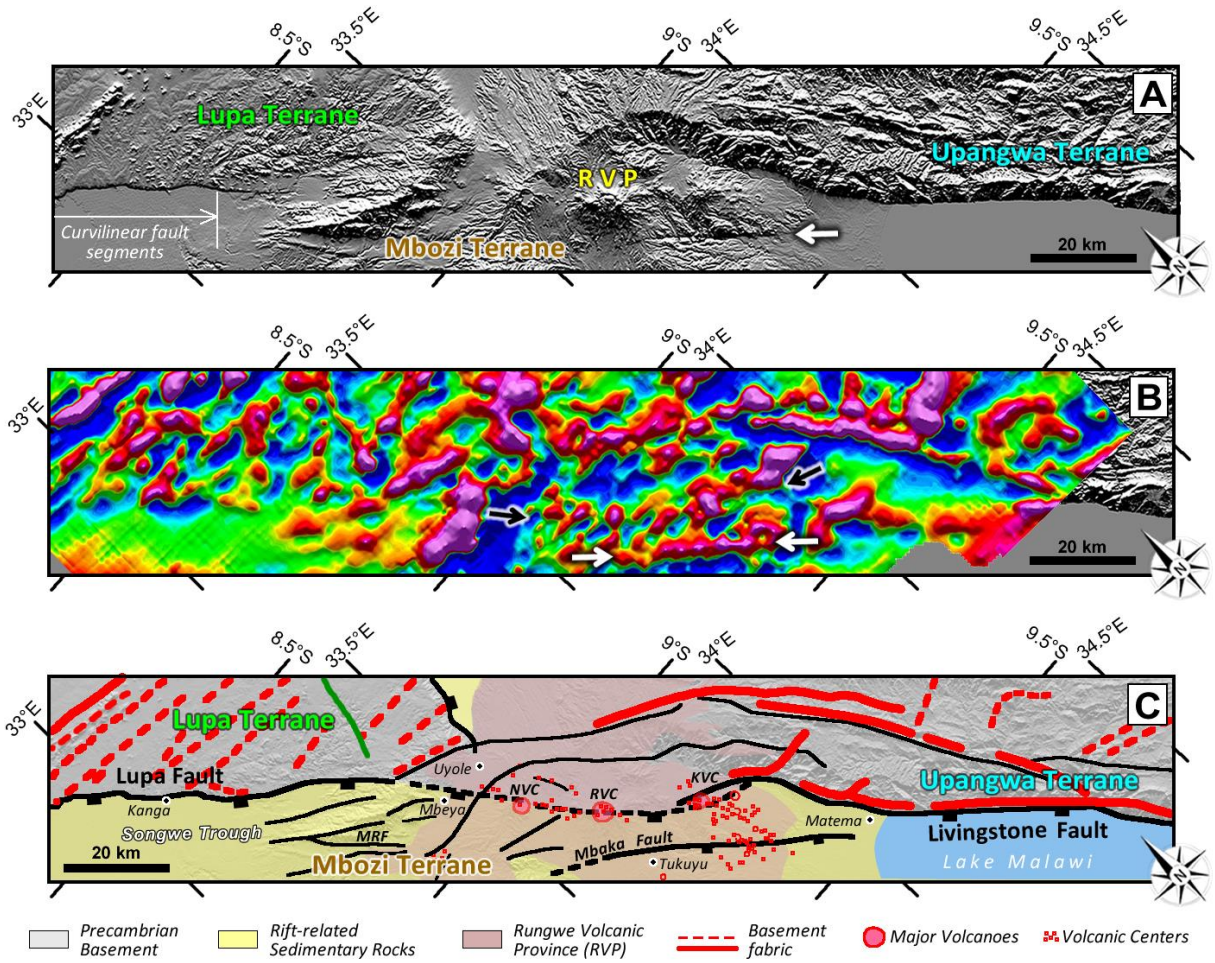

Fig. 11. The southern section of the Lupa Fault, the NE margin of the Mbozi Block (Rungwe Volcanic Province) and a section of the Livingstone Fault (NE border fault if the North Malawi Rift. Topographic digital elevation model in the top panel (A), the vertical derivative of the magnetic data in the middle panel (B), and a structural interpretation in the bottom panel (C). KVC = Kyejo Volcanic Center; NVC = Ngozi Volcanic Center; RVC = Rungwe Volcanic Center. Volcanic centers from Fontijn et al. (2010, 2012).

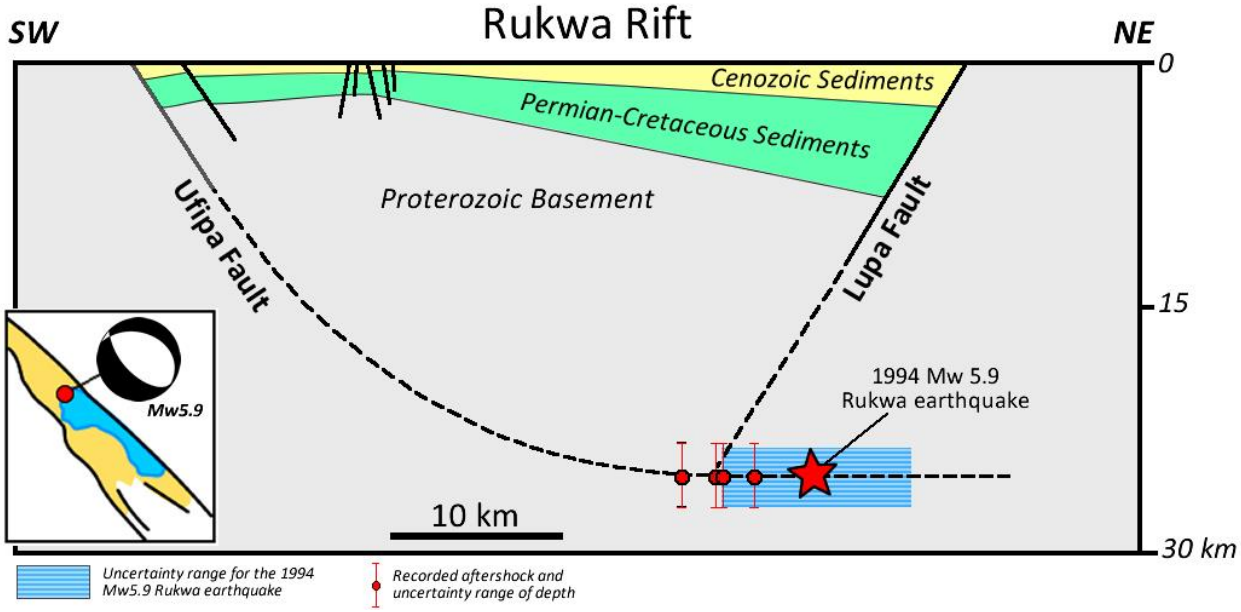

Fig. 12. Generalized geometrical relations of stratigraphic units and normal faults of the Rukwa rift, showing thickening of Cenozoic sediments towards both the Lupa and Ufipa border faults (modified after Zhao et al., 1997).

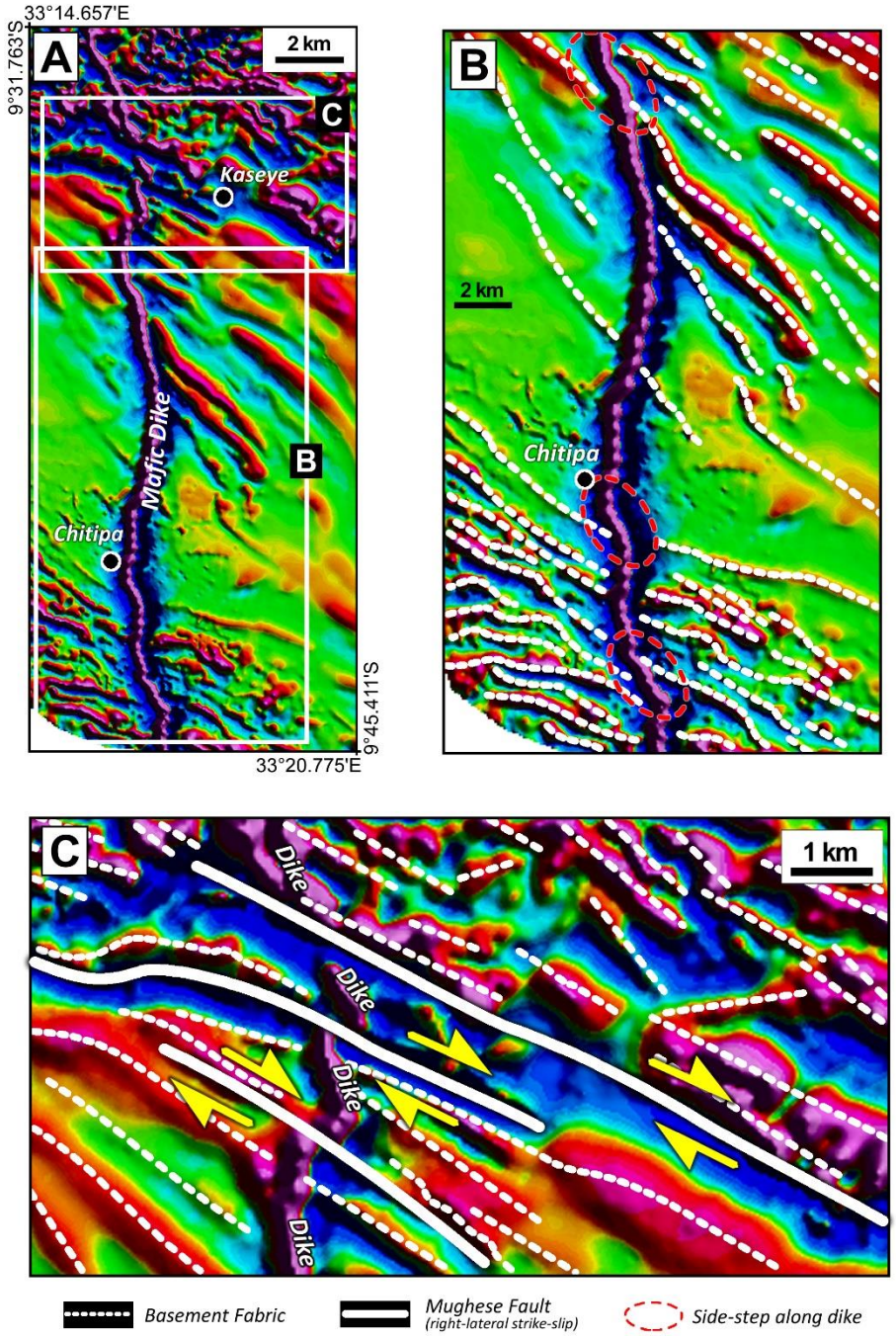

Fig. 13. (A) 1st vertical derivative of the aeromagnetic data covering the Kaseye-Chitipa area along the SW margin of the Mbozi Block (see location in Fig. 8C). (B) Close-up of the central and southern segments of a buried mafic dike (the "Chitipa Dike") showing side-stepping segments that coincide with pre-existing basement fabric. (C) Close-up of the northern segment of the dike showing right-lateral offsets by the continuation of the Ufipa Fault. This strike-slip fault segment is here-in referred to as the Mughese Fault.

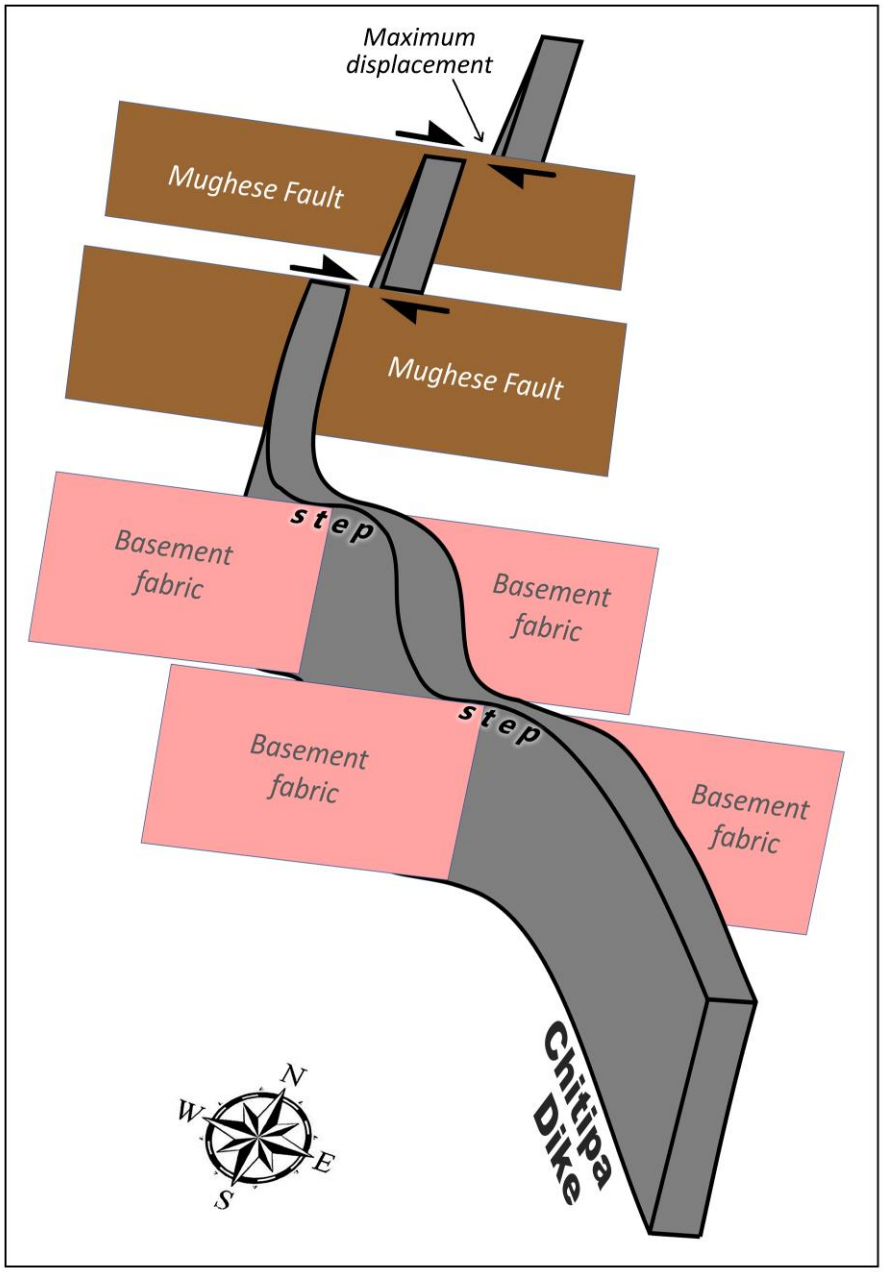

Fig. 14. 3-dimensional (3-D) conceptual model of the geometry of the interpreted dike (the "Chitipa Dike") and its interactions with the pre-existing basement fabric and the post-emplacement Mughese strike-slip fault offset.

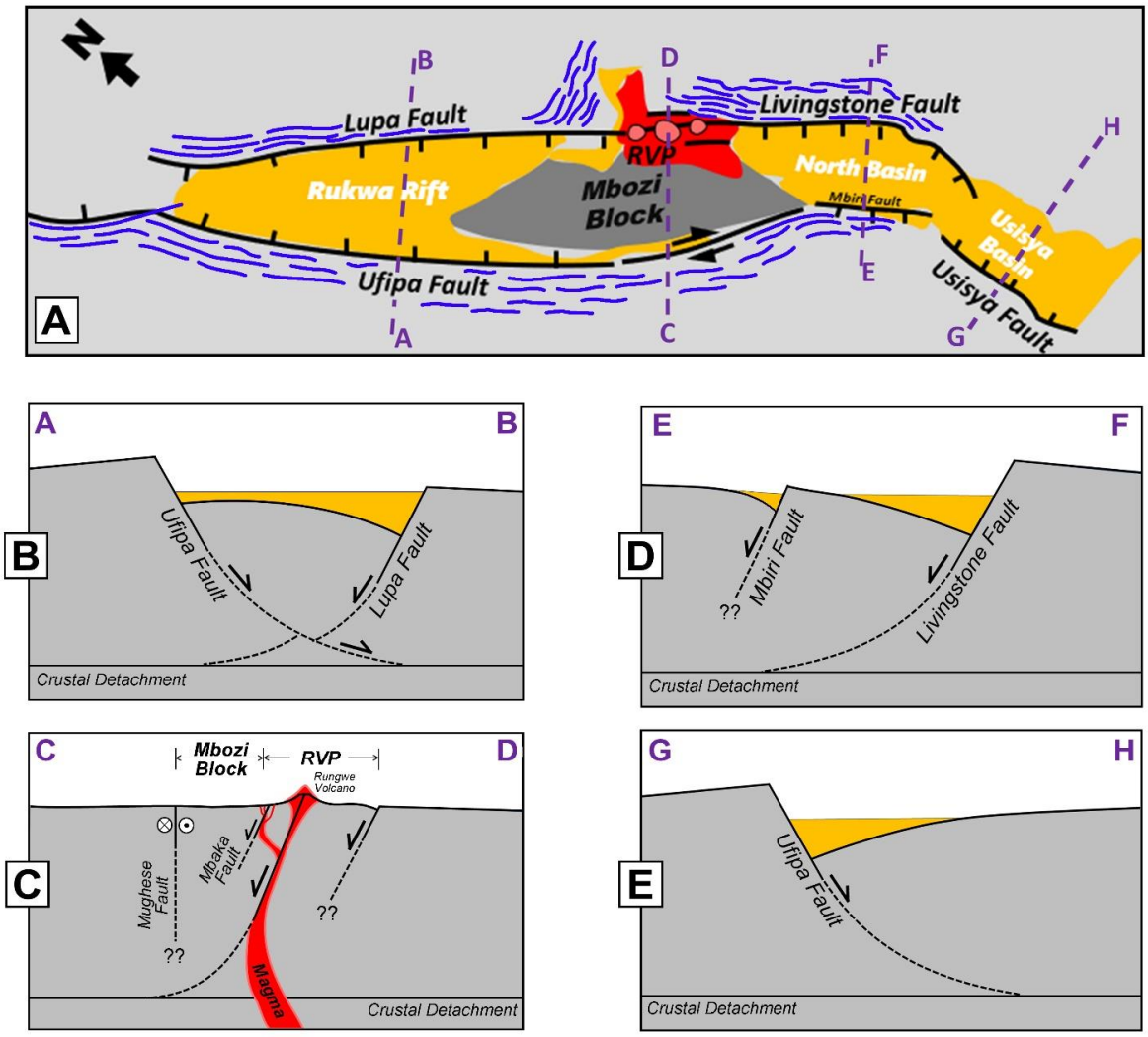

Fig. 15. (A) Generalized cartoon (map view) of the Rukwa-North Malawi Rift Segment (RNMRS) illustrating the continuous structural connectivity along the northeast and southwest boundaries, guided by the basement fabric. Black solid line = fault, blue solid line = basement fabric. RVP = Rungwe Volcanic Province. (B-E) Cross-section cartoons across the segments of the RNMRS, illustrating the possible subsurface geometries and interactions of the domain-bounding structures. LLF = Livingstone-Lupa Fault.

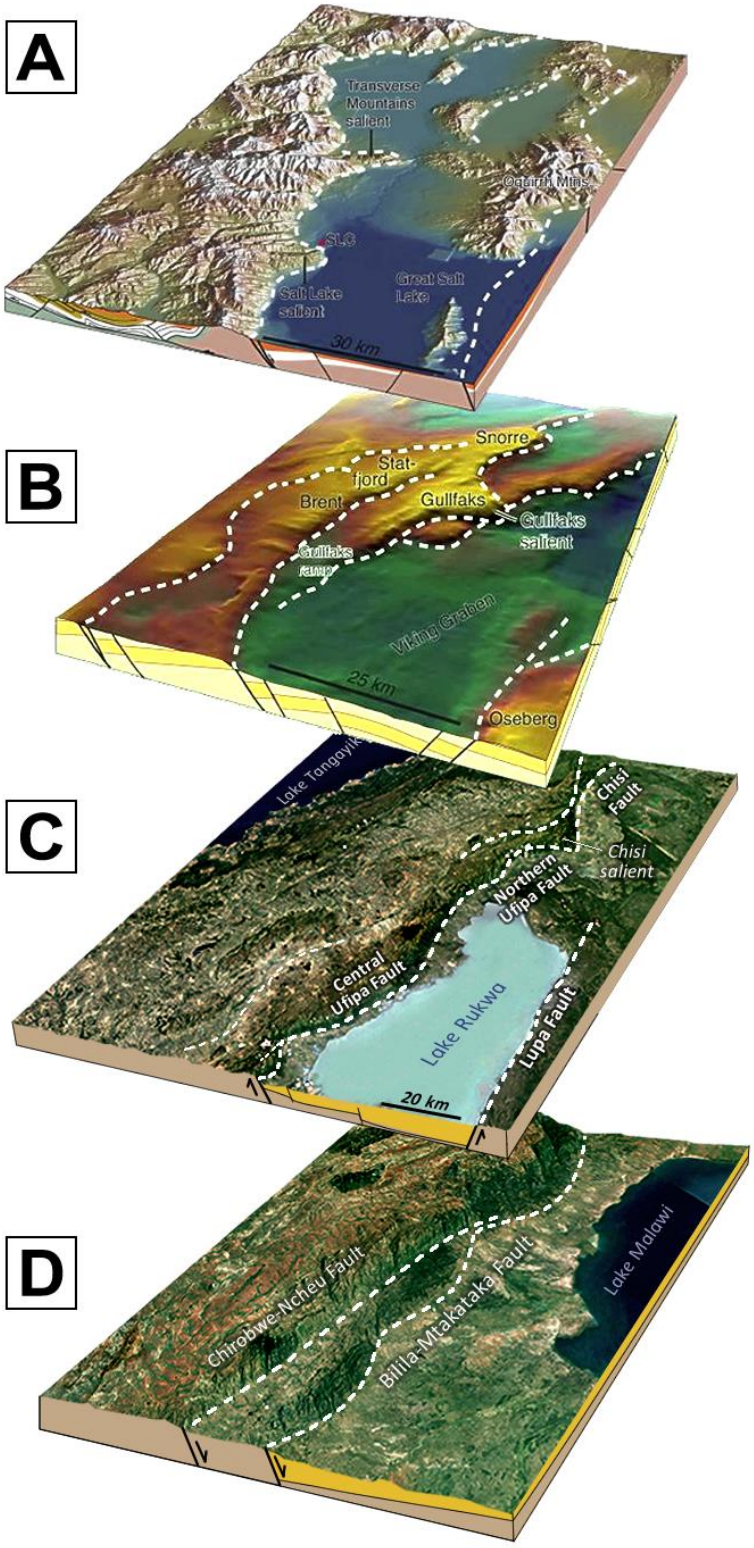

Fig. 16. (A-B) The Wasatch Fault in the Salt Lake area, Utah, and the first-order faults in the northern North Sea (base Cretaceous unconformity) showing concave-curvilinear fault geometries (modified after Fossen and Rotevatn, 2016). (C) Strikingly similar Concave-curvilinear fault geometry occurs in the northern Ufipa Fault and Chisi Fault in the Rukwa Rift. However, the Central Ufipa Fault shows convex-curvilinear fault geometry. (D) The Bilila-Mtakataka Fault also shows excellent convex curvilinear fault geometries.

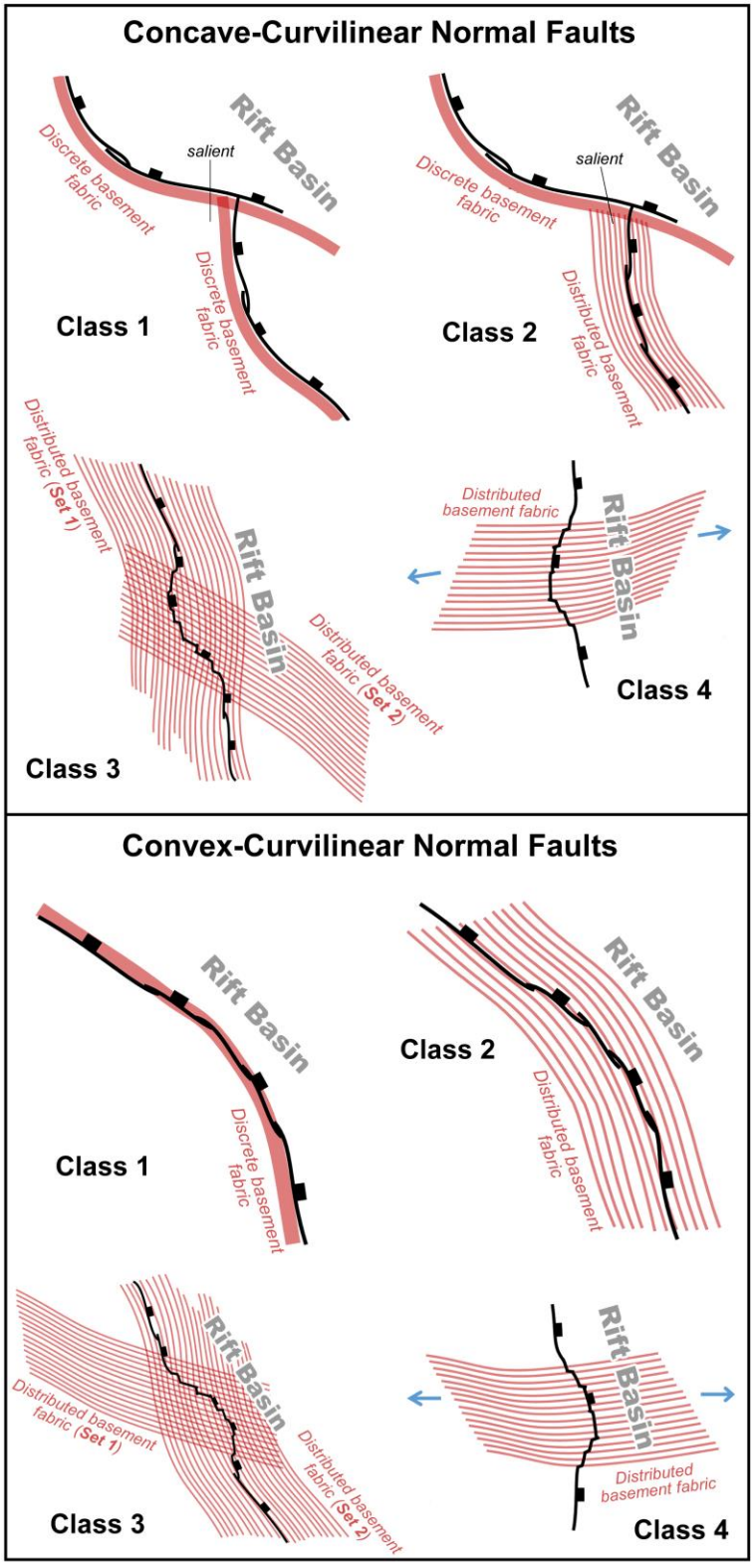

Fig. 17. Models illustrating the control of varying configurations of pre-existing basement fabrics on the development of concave- and convex-curvilinear normal fault plan-view geometries. These models are based on the observations from the Rukwa – North Malawi Rift Segment (this study).

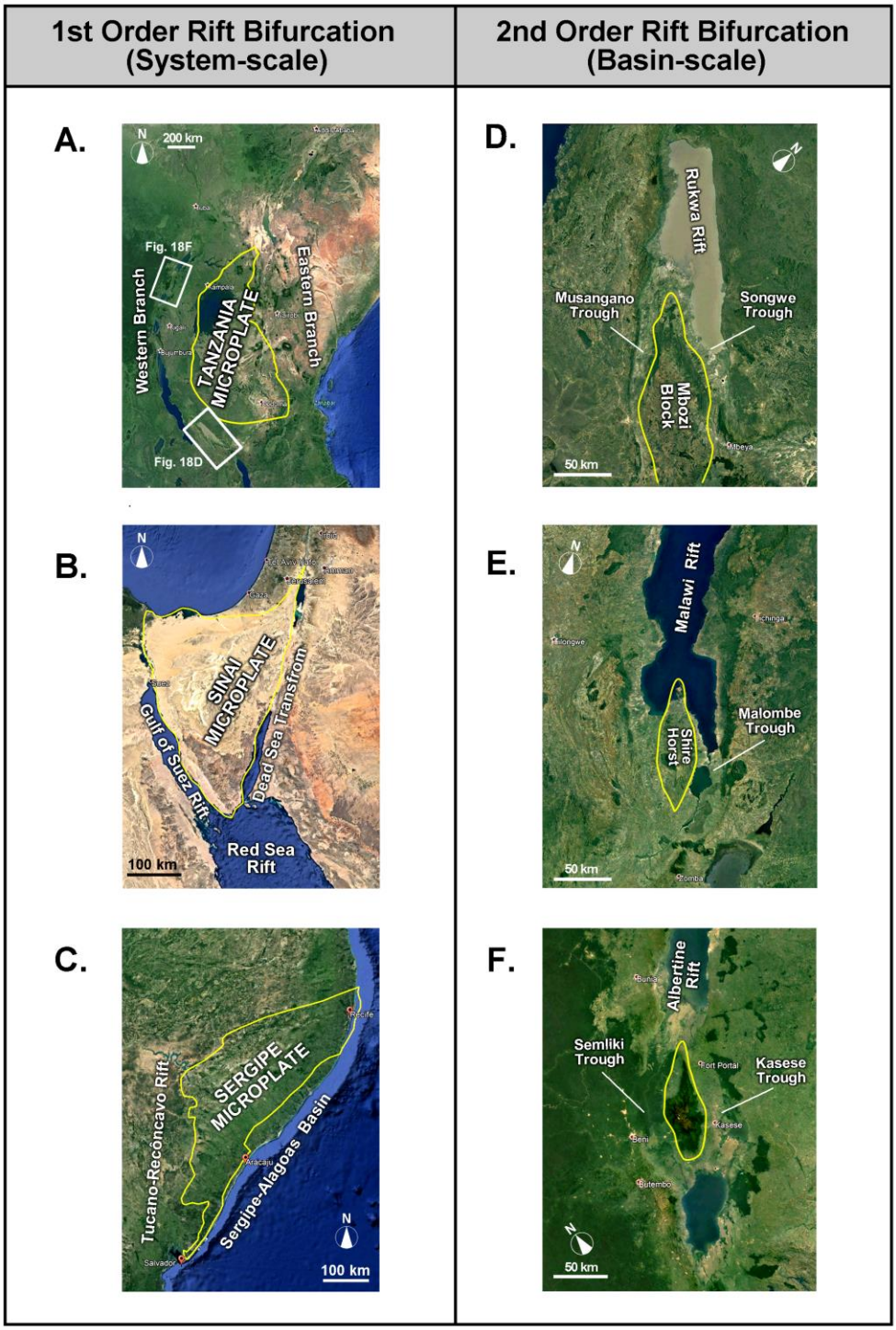

Fig. 18. Examples of system-scale rift bifurcation in the (A) East African Rift System, (B) Red Sea Rift and (C) South Atlantic Rift; and examples of basin-scale rift bifurcation in the (D) Rukwa Rift (see Fig. 18A for location), (E) southern Malawi Rift and (F) Albertine Rift (see Fig. 18A for location). These examples show that the 2nd order bifurcations are integral components of inter-rift transfer zones where the coupling of rift segments take place.